

Ultrawideband Systems and Networks: Beyond C + L-Band

*Original*

Ultrawideband Systems and Networks: Beyond C + L-Band / Hoshida, Takeshi; Curri, Vittorio; Galdino, Lidia; Neilson, David T.; Forsyth, Wlodek; Fischer, Johannes K.; Kato, Tomoyuki; Poggiolini, Pierluigi. - In: PROCEEDINGS OF THE IEEE. - ISSN 1558-2256. - STAMPA. - 110:11(2022), pp. 1725-1741. [10.1109/JPROC.2022.3202103]

*Availability:*

This version is available at: 11583/2975679 since: 2023-02-16T17:41:52Z

*Publisher:*

IEEE-INST ELECTRICAL ELECTRONICS ENGINEERS INC

*Published*

DOI:10.1109/JPROC.2022.3202103

*Terms of use:*

This article is made available under terms and conditions as specified in the corresponding bibliographic description in the repository

*Publisher copyright*

IEEE postprint/Author's Accepted Manuscript

©2022 IEEE. Personal use of this material is permitted. Permission from IEEE must be obtained for all other uses, in any current or future media, including reprinting/republishing this material for advertising or promotional purposes, creating new collecting works, for resale or lists, or reuse of any copyrighted component of this work in other works.

(Article begins on next page)

# Ultra-Wideband Systems and Networks: beyond C+L-Band

Takeshi Hoshida, *Senior Member, IEEE* Vittorio Curri, *Senior Member, IEEE*, Lidia Galdino, *Member, IEEE*, David T. Neilson, *Fellow, IEEE*, Wladek Forysiak, *Member, IEEE* Johannes K. Fischer, *Senior Member, IEEE*, Tomoyuki Kato, *Member, IEEE*, and Pierluigi Poggiolini, *Fellow, IEEE*,

**Abstract**—In the evolution of optical networks, spectral efficiency enhancement has been the most cost-efficient and thus the main driver for capacity enhancement for decades. As a result, the development of optical transport systems has been focused on the C- and L-bands, where silica optical fiber exhibits the lowest attenuation, and erbium-doped fiber amplifiers provide an efficient solution to compensate for the optical loss. With a gradual maturity in the spectral efficiency growth, however, the extension of the optical bandwidth beyond the C+L-band is expected to play a significant role in future capacity upgrades of optical networks and thus attract increasing research interests. In this paper, we discuss the merits and challenges of ultra-wideband optical transport systems and networks beyond conventional bands.

**Index Terms**—Optical communication, wavelength division multiplexing, optical network and switching, ultra-wideband transmission, Raman amplification, optical transceiver, wavelength conversion.

## I. INTRODUCTION

CONTINUOUS efforts to enhance optical transport networks have resulted in a consistent increase of per-fiber capacity exceeding five orders of magnitude over four decades [1]. In core networks, the low-loss wavelength window of a silica-based optical fiber, as shown in Fig. 1, started to be exploited in the 1990s, when wavelength division multiplexing (WDM) technology around the 1550 nm wavelength was deployed along with the erbium-doped fiber amplifier (EDFA) [2–4].

By using gain flattening filters, it was possible to extend the useful frequency range of the EDFA to over 4-THz, and the first WDM band ranging from 1530 nm to 1565 nm, according to Supplement G.sup39 by Telecommunication Standardization Sector of International Telecommunication Union (ITU-T) [5], was named as the conventional band or C-band,

Takeshi Hoshida and Tomoyuki Kato are with Fujitsu Limited, 1-1 Kamikodanaka 4-Chome, Nakahara-ku, Kawasaki 211-8588, Japan (e-mail: hoshida@fujitsu.com; kato.tom@fujitsu.com).

Vittorio Curri and Pierluigi Poggiolini are with Politecnico di Torino, 10129 Torino, TO, Italy (e-mail: vittorio.curri@polito.it; pierluigi.poggiolini@polito.it).

Lidia Galdino is with University College London, Torrington Place, London WC1E7JE, U.K. (e-mail: l.galdino@ucl.ac.uk).

David T. Neilson is with Nokia Bell-Labs, 600 Mountain Avenue, Murray Hill, NJ 07974, USA (e-mail: david.neilson@nokia-bell-labs.com).

Wladek Forysiak is with the Aston University, Birmingham B4 7ET, U.K. (e-mail: w.forysiak@aston.ac.uk)

Johannes K. Fischer is with the Fraunhofer Institute for Telecommunications Heinrich-Hertz-Institute, Einsteinufer 37, 10587 Berlin, Germany (e-mail: johannes.fischer@hhi.fraunhofer.de).

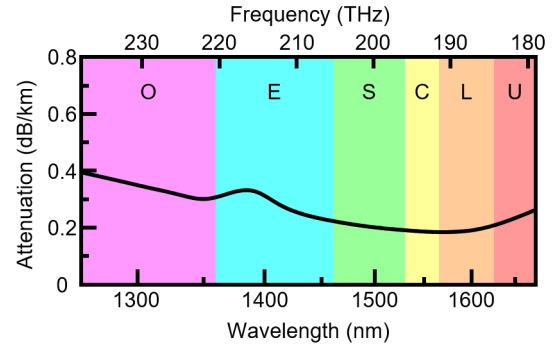


Fig. 1. Low-loss window of the transmission fiber. Horizontal axis is linearly scaled in frequency. Letters indicate band labels.

TABLE I  
BAND DEFINITION

Band	Wavelength range	Bandwidth in frequency
O	1260–1360 nm	17.5 THz
E	1360–1460 nm	15.1 THz
S	1460–1530 nm	9.4 THz
C	1530–1565 nm	4.4 THz
L	1565–1625 nm	7.1 THz
U	1625–1675 nm	5.5 THz

which also corresponds to the minimum loss in a silica fiber. This was quickly followed by the commercialization of the long wavelength band or L-band, ranging from 1565 nm to 1625 nm, in the early 2000s. This was partly to double the number of WDM channels supported by a fiber strand but was also to deploy WDM systems on dispersion-shifted fiber infrastructures, which are known to induce severe crosstalk due to the four-wave mixing (FWM) among WDM channels in C-band running on the same fiber, especially in direct detection [6, 7]. Research toward further exploitation of the low-loss spectral window followed, including S-band (ranging from 1460 nm to 1530 nm), E-band (1360 nm to 1460 nm), O-band (1260 nm to 1360 nm), and U-band (1625 nm to 1675 nm) [8–13].

However, these efforts have not resulted in immediate deployment because they have not been found to be more efficient compared with the other means to increase capacity: dramatic enhancement of spectral efficiency (SE) was developed by the invention of digital coherent transceivers in the late 2000s, i.e., denser WDM with narrower channel spacing

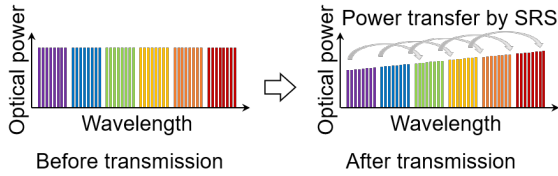


Fig. 2. Schematic diagram of changes in the optical spectrum due to SRS in fiber without wavelength-dependent loss.

and higher-order modulation formats that carry more bits per symbol than previously deployed in 10 Gb/s direct detection systems. After more than a decade of continuous sophistication in digital coherent transceiver technology, however, the improvement of spectral efficiency finally started to show a gradual slow-down of its pace as it approaches to the Shannon capacity [14]. The extension of the wavelength band is thus becoming attractive again and resulted in efforts to extend the bandwidth of the amplifiers for C-band [15] and L-band systems [16], the deployment of numerous C+L-band systems [17–19], and the investigation of ultra-wideband (UWB) systems<sup>1</sup> beyond C+L-band by various organizations.

Challenges toward the development of practical UWB systems reside in several aspects. The first and simplest issue is the wavelength dependence of fiber parameters such as loss, chromatic dispersion, and effective area, which could be approximated as constants in conventional systems. In addition, nonlinear interaction among WDM channels due to FWM, cross-phase modulation, and stimulated Raman scattering (SRS) in a transmission fiber impacts the channel characteristics [20–24]. SRS is particularly important in the context of a UWB transmission. Optical signals at the shorter wavelength (higher frequency) side of the spectrum are affected by the power transfer to the ones at the longer wavelength (lower frequency) side, resulting in the optical signal power of each channel deviating within the UWB signal spectrum considerably (Fig. 2). A possible alternative to single-mode fibers (SMFs) for future UWB systems is hollow-core fibers (HCFs), in particular, the nested antiresonant nodeless fiber (NANF) [25]. Such fibers might provide a very wide bandwidth (300–400 nm) with attenuation comparable to SMF in C-band [26], together with a low dispersion and very low nonlinearity, including SRS. However, this is a very new technology that still needs substantial development to prove commercially viable. In addition, it requires the deployment of a completely new cable infrastructure.

The remainder of the paper starts with a discussion on the modeling of a UWB system including such peculiarities in Section II. Then, we review the state-of-the-art of UWB system demonstrations as well as their enabling techniques in Section III. Section IV discusses the implications of UWB systems in optical networking and node configuration, which is followed by related enabling technologies such as optical switching, optical amplification, mitigation of UWB transceiver impairments, whole band wavelength conversion, and transmission in HCF.

<sup>1</sup>Many publications alternatively use the term multi-band systems instead. In this contribution we use the term UWB systems synonymously.

## II. MODELING OF UWB TRANSMISSION SYSTEM

In this section, we address the peculiarities in modeling a multi-span WDM optical fiber transmission over a bandwidth exceeding the state-of-the-art C-band, and exploiting dual-polarization multilevel modulation formats with a digital signal processing (DSP) based adaptive receiver—the so-called coherent optical technologies. The effect of WDM fiber propagation on such transmission technologies has been extensively analyzed in recent years, and several mathematical models of the physical effects have been proposed and validated. All derivations apply a perturbative approach and aim at describing the nature of the residual impairments after the equalized coherent receiver [27, 28]. These mathematical models can be subdivided into two main families: (a) models aiming at the evaluation of the worst-case effect independently induced by each fiber span and modulation format agnostic: disaggregated models such as the incoherent GN-model [29]; (b) those targeting the entire optically amplified line considering spatial transients and modulation format dependence: aggregated models, such as those of [30, 31] and their evolutions. Models (a) are used in the planning and control of dynamic transparent networks where a disaggregated approach is needed [32], while models (b) enable to optimize point-to-point optical links in both long-haul and short-reach scenarios; for instance, in submarine cables and inter-data-center connections. Independently of the specific approach, all theoretical derivations show that the effect of WDM fiber propagation can be summarized by introducing a disturbance caused by the nonlinear Kerr effect interacting with the chromatic dispersion and attenuation: the nonlinear interference (NLI). Such a disturbance, considered after the full chromatic dispersion compensation applied by the adaptive receiver together with the matched filter and the carrier phase recovery, at the optimal sampling time, has been extensively demonstrated to be well characterized as a dual-polarization additive Gaussian random process. In addition to the NLI, the other disturbance introduced by an optical line is the accumulated amplified spontaneous emission (ASE) noise from the optical amplifiers, which is well modeled as an additive dual-polarization Gaussian random process. Consequently, every transparent lightpath (LP) can be effectively modeled as a dual-polarization additive white and Gaussian noise (AWGN) nonlinear channel [33] characterized by its signal-to-noise ratio (SNR) [34–36]. Because of the presence of nonlinear interference, the LP SNR is typically defined as *generalized* optical SNR (GNSR) and is defined for the  $i$ -th WDM channel as

$$GNSR_i = \frac{P_i}{P_{ASE,i} + P_{NLI,i}}, \quad (1)$$

where  $P_i$  is the received channel power and  $P_{ASE,i}$  and  $P_{NLI,i}$  are the accumulated ASE noise and NLI, evaluated over a bandwidth equal to the symbol rate ( $R_s$ ), respectively [35]. As the LP is a nonlinear channel, its GSNR can be maximized by properly setting the power per channel at the input of fiber spans [37]. The AWGN model for LPs has been extensively proven to be accurate, also in commercial scenarios, using different modulation formats and on mixed fiber types with a chromatic dispersion down to 2 ps/nm/km,

using state-of-the-art symbol rates, or larger [34, 38]. This approach allows to apply the Shannon theory [14] to the WDM optical transmission, so the capacity limit of a WDM comb over an amplified fiber link can be defined as:

$$C = 2 \sum_{i=1}^{N_{ch}} R_{s,i} \log_2(1 + GSNR_i) \left[ \frac{\text{bit}}{\text{sec}} \right], \quad (2)$$

where the factor 2 accounts for the dual-polarization and  $R_{s,i}$  and  $GSNR_i$  are the symbol rate and GSNR for the  $i$ -th WDM channel, respectively. To better show the need for additional spectrum to enlarge the link capacity, it is useful to focus on the simplified scenario of a fixed WDM grid  $\Delta f$  and uniform symbol rate  $R_s$  together with a flat GSNR. Therefore, Eq. 2 is simplified to  $C = 2 B (R_s/\Delta f) \log_2(1 + GSNR)$ , where  $B = N_{ch} \Delta f$  is the total transmission bandwidth. State-of-the-art transceivers are very close to the limit [39], thanks to  $R_s/\Delta f$  approaching the unit (e.g.,  $R_s = 69$  GBd in  $\Delta f = 75$  GHz), the rate flexibility enabled by hybrid formats [40] and shaped constellations [41]. Some further capacity can be obtained by using hybrid EDFA/distributed Raman amplification [42] and/or using DSP techniques to partially compensate for the NLI [43], which increases the optimal GSNR, but the effect on the capacity of larger GSNR levels is limited by the logarithmic law. Therefore, to obtain more capacity, the total transmission bandwidth  $B$  must be enlarged, either by activating a new fiber line, or by exploiting additional bands on the same fiber line, as proposed in this work.

The available mathematical models for the NLI generation can be extended to their use on the UWB transmission from the O- to the U-band, with the exception of a guard band around the zero-dispersion wavelength that is in the O-band for standard SMF (SSMF). The requested guard band width depends on the minimum tolerable chromatic dispersion by the transmission technique, channel spacing, and power levels used in the spectral region. Moreover, the statistics of the zero-dispersion wavelength that may vary fiber by fiber is relevant in defining the guard band. Later, we will comment on the modeling transmission close to the zero-dispersion wavelength.

In UWB scenarios, the wave equation governing the evolution of the modal amplitude in the SMF is the same coupled nonlinear Schrödinger equation (CNLSE) as that for the C-band analysis because the fiber is in the single-mode regime and nonlinearities are perturbations on the entire O-to-U-band spectrum [20]. Note that in general the CNLSE is a stochastic equation, as it includes the random birefringence. Focusing on the analysis of propagation of dual-polarization coherent optical technologies, the propagating optical signal is depolarized over short propagation distances, so we can apply a polarization average to the wave equation. Moreover, the polarization mode dispersion (PMD) is typically compensated for by adaptive coherent receivers and weakly interacts with NLI generation. Consequently, we can assume the fiber wave equation to be the Manakov equation [44] centered at the wavelength of the channel under test. The WDM spectrum is the comb of the dual-polarization spectrally orthogonal  $N_{ch}$ , which are statistically independent random processes.

Substituting such a signal form in the Manakov equation, we obtain a set of  $N_{ch}$  wave equations, each including loss, chromatic dispersion, and self- and cross-channel nonlinear effects: the spectrally separated Manakov equation (SSME). Nonlinear effects are always a perturbation, so each channel is assumed to propagate in accordance with the following perturbative law:

$$\bar{A}_i(f, z) = \{\bar{A}_i(f, 0) + \bar{N}_i(f, z)\} \sqrt{p_i(z)} H_{D,i}(f, z), \quad (3)$$

where  $f$  is the frequency and  $z$  is the propagation distance.  $\bar{A}_i(f, z) = [A_{x,i}, A_{y,i}]^T$  is the optical field amplitude of the  $i$ -th channel under test,  $p_i(z)$  is the power evolution including loss and SRS [23, 24] effects,  $H_{D,i}(f, z)$  is the effect of chromatic dispersion, and  $\bar{N}_i(f, z) = [N_{x,i}, N_{y,i}]^T$  is the NLI spectrally centered on the  $i$ -th channel. Substituting Eq. 3 in the SSME, the set of differential equations is obtained for the generation of the  $N_{ch}$   $\bar{N}_i(f, z)$  components. Integrating the equations and relying on the statistical properties of digital signals, the power spectral density  $G_{N,i}(f)$  of  $\bar{N}_i(f, z)$  can be evaluated. The coherent receiver applies the matched filter, so the intensity of the NLI Gaussian random process impairing the decision signal is  $P_{NLI,i} = \int_{-\infty}^{+\infty} G_{N,i}(f) |H_m(f)|^2 df$ . Different mathematical models proposed in the literature rely on different approaches and approximations for the  $P_{NLI,i}$  calculation, but all can be summarized in the following common form:

$$P_{NLI,i} = \eta_{SPM,i} P_i^3 + P_i \sum_{j \neq i} \eta_{XPM,ij} P_j^2 + \sum_{klm \in FWM_i} \eta_{FWM,iklm} P_k P_l P_m, \quad (4)$$

where  $P_i$  is the input power of the  $i$ -th channel,  $FWM_i$  is the set of FWM indices  $klm$  on the  $i$ -th channel, and  $\eta_{SPM,i}$ ,  $\eta_{XPM,i}$ , and  $\eta_{FWM,iklm}$  are the efficiencies for self- and cross-phase-modulation, and FWM, respectively, which generate the self-, cross-, and multi-channel NLI components, respectively. For most practical scenarios, FWM is negligible, so the NLI components can be spectrally separated. Aggregated mathematical models focus on computing the overall NLI generated by the optical link by integrating the differential equation for  $\bar{N}_i(f, z)$  on the entire transmission system, while the disaggregated NLI models aim at the evaluation of the equivalent NLI generated by each fiber span.

In UWB scenarios, contrary to the C-band analyses, typical approximations in fiber parameters must be removed to properly take into account frequency dependencies across the wide bandwidth, starting with variations in the frequency of loss and chromatic dispersion [20]. The Kerr effect can still be considered as instantaneous [45], while scaling with the wavelength  $\lambda$  of the channel under test in the effective area, and consequently that of the nonlinear coefficient  $\gamma$ , must be included [20].

Specifically, variations with  $f$  of loss must be accurately considered. An effective method to properly consider variations with  $f$  of loss is to rely on the phenomenological expansion proposed in [46]:

$$\alpha(\lambda) \simeq \alpha_S(\lambda) + \alpha_{UV}(\lambda) + \alpha_{IR}(\lambda) + \alpha_{13}(\lambda), \quad (5)$$



where  $\alpha_S(\lambda)$ ,  $\alpha_{UV}(\lambda)$ ,  $\alpha_{IR}(\lambda)$ ,  $\alpha_{13}(\lambda)$  are the Rayleigh scattering, ultraviolet, infrared, and  $\text{OH}^-$  peak absorption contributions, respectively. In [47], it has been experimentally shown as this phenomenological approach is effective and needs to define only four parameters for an accurate and reliable loss profile model.

The SRS has a negligible effect on the modulation time constant [48], so its practical impairment on WDM signal combs is a seamless transfer of optical power from higher to lower frequencies depending on the frequency spacing  $\Delta f$ , with the efficiency peak of  $\Delta f$  around 12 THz [49, 50]. This means that the SRS can be considered a power-dependent spectral tilt for the C-band-only transmission. While, in the case when the fiber spectral exploitation approaches or exceeds 12 THz, the effect of SRS on per-channel power evolution must be accurately evaluated [51] given the power spectral density at the fiber input by solving the SRS set of  $N_{ch}$  differential equations [24, 52]:

$$\begin{aligned} \frac{\partial P_n(z)}{\partial z} = & -\alpha_n P_n(z) + \\ & -P_n(z) \sum_{m=1}^{n-1} C_R(f_n; \Delta f_{nm}) P_m(z) + \\ & +P_n(z) \sum_{m=n+1}^{N_{ch}} C_R(f_m; \Delta f_{mn}) P_m(z) \quad (6) \end{aligned}$$

where  $P(z)$  is the power evolution of the  $n$ -th channel centered at  $f_n$  in the  $N_{ch}$  WDM channel comb,  $\alpha_n$  is the loss coefficient for the  $n$ -th channel,  $\Delta f_{nm} = f_n - f_m$  and  $C_R(f_n; \Delta f_{nm})$  is the Raman efficiency referring to  $f_n$  for the spectral separation  $\Delta f_{nm}$ . Note that to achieve an accurate evaluation of SRS, a proper shape for the Raman profile and its scaling with a reference frequency must be considered [49, 51].

Given the input power per channel  $P_n = P_n(0)$ , the solution of Eq. 6 is the per-channel power evolution  $P_n(z) = P_n \cdot p_n(z) = P_n \exp(-\alpha_n z) G_{SRS,n}(z)$ . To show the effect of SRS, as shown in Fig. 3 the UWB loss modified by the SRS over 70 km of the SSMF without  $\text{OH}^-$  absorption (ITU-T G.652D fiber) is depicted together with the intrinsic fiber loss. The full spectral load ( $\Delta f = 75$  GHz,  $R_s = 64$  GBd) from O- to U-band is considered and the input power per channel has been optimized to maximize the GSNR without considering the effect of SRS. A simple flat single-band power optimization on each per-band center channel [37] has been applied. To better focus on the effect of fiber, amplifiers are considered ideal with noise figures (NFs) [19] of 7 dB for the S- and O-bands, 6 dB for the E-, L-, and U-bands, and 5.5 dB for the C-band. Using these hypotheses, Eq. 6 has been solved on the O-to-U band, considering the loss  $\alpha(f_n)$  and Raman  $C_R(f_n; \Delta f_{nm})$  profiles of the SSMF, including the Raman efficiency scaling with  $f_n$  [49]. Results are shown in Fig. 3 where it can be observed that all higher frequencies for which the overall spectrally occupied lower frequencies exceed the Raman peak—roughly the O- to S-band—experience an extra loss due to SRS depletion. In contrast, with a change of regime in the C-band, frequencies without an occupied spectrum exceeding the SRS peak at lower frequencies experi-

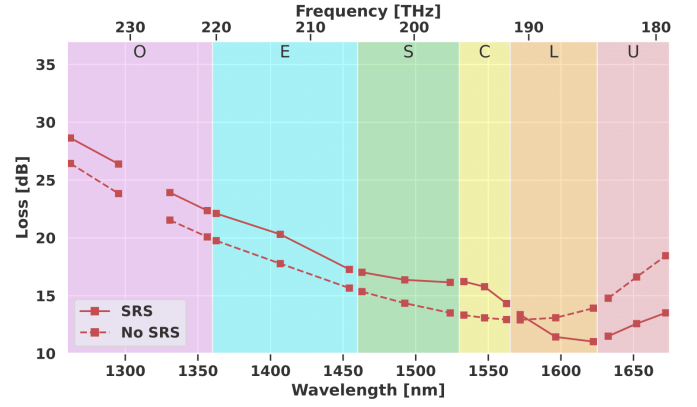


Fig. 3. Loss introduced by 70 km of the SSMF: fiber loss only (dashed) and fiber loss including the SRS effect (solid). Flat per-band input power per channel optimized without SRS.

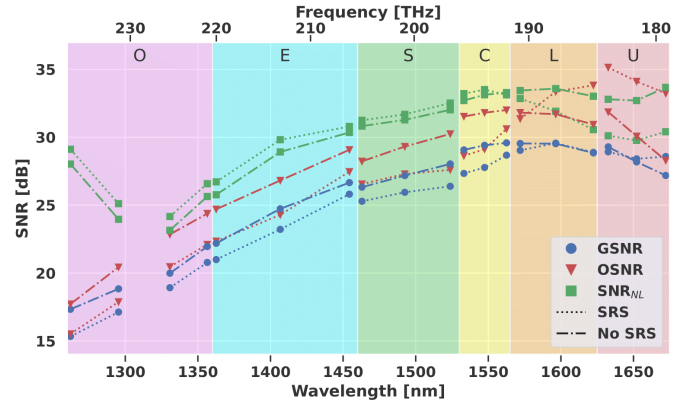


Fig. 4. GSNR(blue) with and without the SRS effect, together with OSNR (red) and  $\text{SNR}_{NL}$  (green) components, by 70 km of the SSMF. Flat per-band input power per channel optimized without SRS.

ence a loss reduction due to SRS enhancement. Therefore, the SRS is the main UWB effect that, depending on the overall spectral load, enlarges loss at larger frequencies, enhancing the ASE noise impairments and reducing the NLI. The opposite occurs for lower frequencies, for which the SRS enhancement mitigates loss, and therefore, reducing the effect of ASE noise and enhancing the NLI generation. These UWB effects must be accurately considered in the mathematical NLI models when applied to ultra-wideband scenarios, otherwise they rapidly lose accuracy with the expansion of spectral occupation beyond the C-band. So, mathematical models for the NLI generations must be adjusted by including the per-channel power profile  $P_n(z)$  obtained by solving the SRS equations 6. For instance, the generalization of the GN-model by including the SRS and loss profile has been proposed and validated in [36, 53, 54].

To observe the impact of the UWB loss profile and that of SRS, in Fig. 4 we display the GSNR and its optical SNR (OSNR) and  $\text{SNR}_{NL}$  components evaluated [36] on the 70-km scenario considered for the loss plots of Fig. 3. These results have been obtained considering typical SSMF chromatic dispersion and loss profiles with respect to the frequency [19]. The fiber effective area is supposed  $80 \mu\text{m}^2$

in the C-band scaling with the inverse of the frequency in the other bands [49]. As expected, if we do not include the SRS (dot-dashed curves), the OSNR component is always 3 dB lower than the  $\text{SNR}_{NL}$  at each band center frequency. The scenario drastically mutates when properly considering the SRS in evaluating the GSNR and its components. By analyzing these results shown in Fig. 4 (dotted curves), it is evident how the SRS depletion impacts O-to-S bands by reducing the OSNR and enlarging the  $\text{SNR}_{NL}$ . Therefore, these bands operate in almost a linear regime with the GSNR defined by the OSNR— $\text{SNR}_{NL}$  practically negligible—and reduced by 1–2 dB with respect to the prediction without considering the SRS. The opposite occurs for the L- and U-bands that are forced to operate in the nonlinear regime. For these bands, the GSNR is not reduced because of the strong benefits in the OSNR due to SRS enhancement that compensates for the  $\text{SNR}_{NL}$  reduction. The C-band is the transition from one regime to the other. Practical implications of this behavior are as follows. (i) To properly manage UWB optical transport, the GSNR computation must accurately include the effect of SRS in both OSNR and  $\text{SNR}_{NL}$  computations. (ii) The optical controller setting the amplifiers, and consequently the fiber input power per channel for each band, must be a multi-band optical controller that sets all the per-band amplifiers [55]. (iii) Deploying traffic on additional bands on the same fiber must be accurately controlled to avoid GSNR reduction and, as a result, the possibility of service outages on already active WDM channels.

Finally, we comment on modeling fiber transmission when approaching the zero-dispersion wavelength  $\lambda_{zd}$ . When the chromatic dispersion approaches zero, the nature of the problem is modified, the perturbative approach must be modified as proposed in [56], and relevant parametric phenomena may impact propagation [20]. Moreover, in such a spectral region, considering the statistical variations of  $\lambda_{zd}$  in cables [57] becomes crucial because of possible chromatic dispersion magnitude variations being comparable with its nominal value. So, a clear assessment of nonlinear transmission modeling in such a spectral region has not yet been proposed. From a practical perspective, the stochastic nature of the problem, and consequent possible issues on reliable LP deployment, suggests exploiting the spectral region around the nominal  $\lambda_{zd}$  for short-reach transmission only with the power level kept below the nonlinear threshold.

### III. EXPERIMENTAL DEMONSTRATIONS OF UWB TRANSMISSION AND ENABLING TECHNIQUES

Research in SMF communication systems is currently being driven by two complementary strategies: bandwidth expansion and spectral efficiency enhancement. It is, therefore, unsurprising that high-capacity SMF transmission system demonstrations regularly showcase new communications technologies while providing a key indicator of progress in the field as a whole. Several milestones in the achievable data throughput in SMF [58–69] reported over the past decade are shown in Fig. 5. Particularly, it highlights the different amplification technologies that enabled the transmission bandwidth

beyond the conventional C+L-band. Few efforts have been made to maximize capacity through transmission bandwidth extension in trans-Atlantic ( $> 6,000$  km) and trans-Pacific ( $> 9,000$  km) systems. These transmission systems are electrical power feed constrained, and optical fiber parallelism is seen as a better solution to maximize cable capacity. In contrast, record capacities over short transmission distances have mainly used amplification technologies that extend bandwidth beyond C+L-band EDFAs. In [61], a semiconductor optical amplifier (SOA) with a 100 nm gain bandwidth demonstrated the potential for a SMF capacity of 115.9 Tbit/s over a 100-km transmission distance. The relatively high NF of SOAs versus, for example, EDFAs means they are generally considered unsuitable for repeated transmission systems. Nevertheless, by combining an SOA with distributed backward Raman amplification, a 107-Tbit/s transmission over 300 km ( $3 \times 100$  km) was reported in [63]. In [62] a distributed Raman amplifier with a 11.2-THz bandwidth enabled a 102-Tbit/s transmission over 240 km ( $3 \times 80$  km). An even greater data rate of 120 Tbit/s over 630 km ( $9 \times 70$  km) was shown by using hybrid distributed Raman-EDFA amplifiers with a continuous 91-nm gain bandwidth [64]. Further extension in transmission bandwidth towards lower S-band wavelengths resulted in a higher SMF capacity. In [60], a 150.3-Tbit/s transmission over 40 km was demonstrated. The transmitted signals occupied a total bandwidth of approximately 109 nm (13.625 THz), and a distributed backward Raman amplification scheme for the S-band and EDFAs for the C- and L-bands were used to compensate for the fiber loss. In [59], the combination of a thulium doped fiber amplifier (TDFA), discrete Raman amplifiers and C+L band EDFAs provided a continuous gain bandwidth of 16.83 THz (1484.86–1619.67 nm), achieving a net throughput of 178.08 Tbit/s over 40 km. In [58], a record net data throughput of 190 Tbit/s over 54 km was shown. The channels were transmitted over a gain bandwidth of approximately 17.25 THz, and a hybrid distributed Raman/TDFA for S-band, together with C+L-band EDFAs, was used for signal amplification. Fig. 5 summarizes the transmission performance achievable with state-of-the-art technology under specific conditions. In the design of commercial systems, it is necessary to ensure dynamic range and margin to cope with variations in various parameters such as span loss and aging of components. It is therefore appropriate to understand that these hero experiments are somewhat beyond the upper limits of performance achievable with commercial systems.

A UWB transmission architecture has already been envisioned in [70]. Even though UWB components are still unavailable, powerful experimental laboratory techniques, which permitted savings and massive duplication of equipment, have enabled the experimental demonstration of large-scale WDM systems [1]. For wideband transmissions, different lab approaches to emulate the aggressors channels per band have been demonstrated. In [60], 47 carrier signals from DFB-LD and a I/Q sub-carrier generator were used to generate 84 carrier signals. In [58], a single wideband comb-source generated the interfering carriers across the entire 17.25-THz transmission bandwidth, and a single IQ-modulator was used to modulate all carriers. However, the spectral region of S-band wavelengths

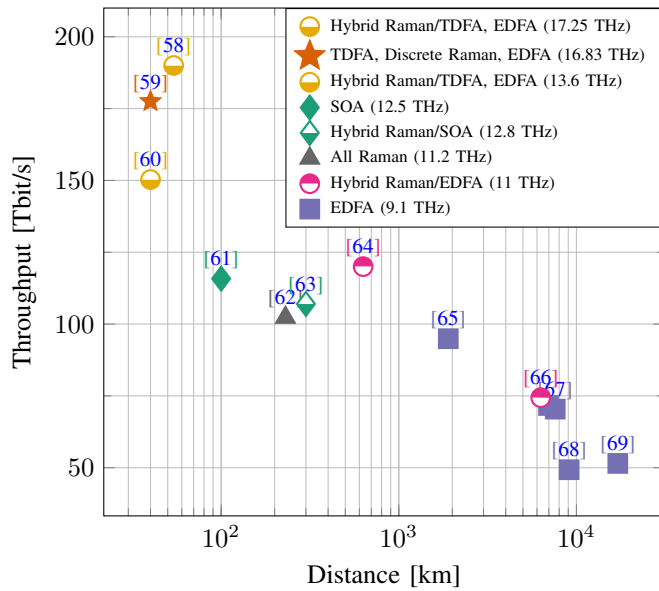


Fig. 5. Record data throughput versus distance for single-mode fiber. The transmission bandwidth indicated in each case is for the usable spectrum, not including spectral gaps between amplifier gain bandwidths.

of the comb had a lower optical power, which contributed to worse channel performance at this band. To overcome this lower optical power per comb line at S-band wavelengths in [71], the same wideband comb-source was used by Puttnam et al. to generate the carriers over only the C- and L-bands, and a single modulator was used to modulate the interfering channels in the C+L bands. The S-band interfering modulated channels were generated by band wavelength conversion from an amplified tap of the L-band modulated channels.

An even simpler technique used to emulate the aggressors' channels, which is valid for high-SE dispersion-unmanaged coherent systems, uses the ASE of optical amplifiers, whose Gaussian optical field statistics accurately emulates a tightly packed broadband multiplex of spectrally and constellation-shaped WDM channels [72, 73]. In [61, 63], a combination of banks of lasers together with ASE noise sources were used to emulate a continuous 12.5 THz bandwidth aggressor channel, while a continuous 11-THz and 16.8-THz ASE noise source was used in [64, 66] and [59], respectively.

Another experimental test-bed architecture solution and commercial product alternative for UWB transmission is whole band wavelength conversion for signal generation and reception proposed in [74]. Details of this new approach are given in Section IV.D.

These laboratory schemes have enabled the experimental demonstration of up to a 17-THz occupied transmission bandwidth, achieved by simultaneously using the S-, C-, and L-bands. However, it is important to note that, to date, for all wideband experimental demonstrations [58–61, 63, 74], the S-band channel wavelengths (< 1530 nm) experienced worse received performance compared with the C- and L-band wavelengths. For instance, Fig. 6 illustrates the information rate and received SNR for all 660 channels at 25-GBd channels after a 40-km transmission (details of the transmission system under investigation can be found in [59]). In this particular sys-

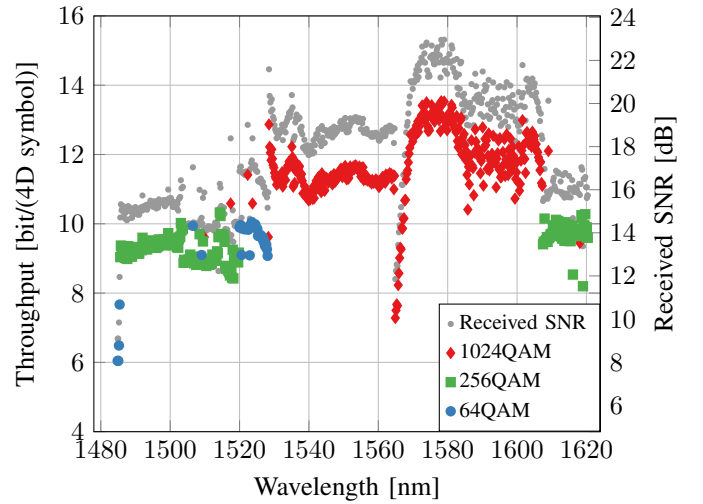


Fig. 6. Per-channel throughput and SNR over two polarizations after 40 km.

tem, the combination of fiber parameters, hybrid amplification method, and different back-to-back implementation penalties per band, lead to a significant SNR wavelength dependence (details are given in Section IV.D and [75]). To mitigate this effect and maximize the achievable information rate (AIR) of each individual channel, new geometrically-shaped (GS) constellations tailored for the SNR of each wavelength were designed and implemented [59]. As can be seen in Fig. 6, in the C- and L-bands, 1024-ary GS constellations were mainly used, while for channel wavelengths < 1530 nm, GS-64QAM and GS-256QAM provided higher AIRs.

To date, only approximately a third of the low-loss window of a single-mode silica fiber bandwidth has been experimentally demonstrated. Notwithstanding seamless amplification technology can be designed and developed, experimentally study a fully-ed 50 THz SMF transmission system in a simplified and inexpensive manner remains a challenge.

#### IV. IMPLICATION OF UWB SYSTEM IN OPTICAL NETWORKING AND SWITCHING

When considering the suitability of UWB systems we must consider the constraints placed on optical systems in different parts of the network. Transoceanic communication cables [76] have often been at the forefront of adopting fiber technologies including EDFA [77]. Because these systems deploy both amplifiers and fiber at the same time, the issue of legacy fiber losses is less problematic. For repeated undersea systems such as transoceanic cables, there is a constraint on total system power and the cross-sectional diameter of the cable. Therefore, increasing available optical bandwidth looks to be promising way to scale cable capacity if broader band optical amplifiers with high efficiency and low NFs can be developed. Expansion of the optical bandwidth can lead to lower power per bit per amplifier by enabling a reduction in the spectral efficiency that results in a larger reduction in power. This is applicable to both UWB and space-division multiplexing approaches.

In terrestrial systems the potential application space may be subject to a different set of constraints. It is likely they will have to operate over an installed fiber, which may limit



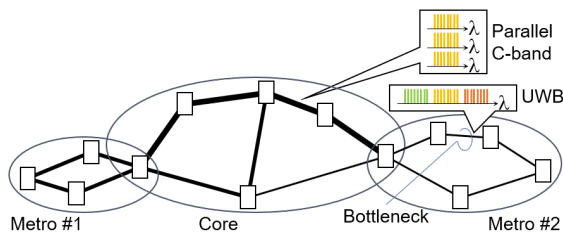


Fig. 7. Schematic diagram for metro/core network based on UWB and conventional dense WDM. For segments with limited fiber availability (shown by thin lines), UWB transmission should be efficient in upgrading the network capacity without a new fiber build, while fiber-rich segments can use parallel conventional systems.

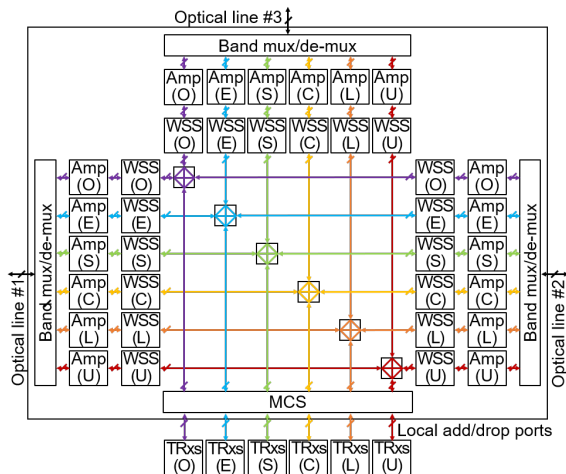


Fig. 8. Exemplified block diagram for UWB 3-degree ROADM node having banded amplifiers, banded WSSs, and UWB multi-cast switches (MCS) connected to banded transceivers (TRxs).

the available spectrum due to higher transmission losses in other bands, as shown in Fig. 1. In longer haul systems (typically greater than 500 km) the fiber span lengths (80–120 km) may cause certain fiber bands, such as O and E, to have unacceptably high losses, unless amplifier spacing were reduced. However, in the metro space, where low latency 5G applications and video streaming may drive rapid growth in demand, fiber spans can be significantly shorter (10–40 km), and much larger fiber bandwidths may become an attractive way to scale capacity on existing fiber plants (Fig. 7). Unlike in early WDM systems where maintaining constant noise performance across the wavelength range was critical for system capacity, today’s coherent transponders enable the capacity to be adjusted on the basis of the noise and impairments of each particular channel. This somewhat alleviates the need for constant losses and NFs from each amplifier or band.

To support the UWB network, it is necessary to expand the wavelength coverage of network elements such as transceivers, in-line amplifiers, and switch nodes such as the re-configurable optical add-drop multiplexer (ROADM) or wavelength cross-connect. The actual node configuration that supports the UWB network should be designed in view of the limitations of practical optical components and subsystems. Fig. 8 shows one possible configurations for a 3-degree ROADM node, having a transmission fiber in/out of 3 directions and local

add/drop ports to be interfaced with transponders. In this example, the input/output interfaces to the transmission fibers are with wavelength-band multiplexers and demultiplexers so that different types of amplifiers and wavelength selective switches (WSSs) are used in parallel to amplify and switch different portions of the UWB spectrum. The local add/drop port adopts a single UWB multi-cast switch so that any transponder connected to any port can be routed from/to the appropriate WSS with the intended band and direction. Note that the node should become simpler if a single amplifier and/or a single WSS can handle multiple band signals together. In the following subsections, several key technologies to support the future evolution of UWB networking are provided. For complementary and detailed discussions on the UWB devices and subsystems, the readers are also encouraged to look into another paper in this special issue [78].

### A. Wavelength Switching

Current wavelength switching architecture [79] consists of using WSSs to build mesh-connected nodes with the option to add and drop local traffic. Internally, a WSS is an optical system that forms a spectrometer that disperses the light across a switching element, which is used to switch selected wavelengths to the needed output ports. The spectrometer is constructed using lenses, mirrors, gratings, and polarization optics, and the switching element is typically a liquid crystal on silicon (LCoS) reflective phase modulator, which is used to create holograms that steer portions of the spectrum to different ports. In current optical transport systems, a WSS typically covers either the C or L-band and typically has 20 or more optical output ports, to enable mesh connections, and so a C+L system will typically have a band splitter and two WSSs per fiber. If this approach is used to open up additional spectral bands, as shown in Fig. 8, this introduces the same system switching complexity as using more fibers. The technologies for constructing WSSs can be adapted to operate in different wavelength bands [80] or over larger (36 THz) optical spectra [81], with the recent commercial implementation of 10 THz [82]. There are a number of constraints on the functionality as the switches are scaled to larger bandwidths. The spectral resolution of a WSS is limited by a combination of the spectrometer resolution, which is determined by the number of lines of the grating that is illuminated and by the number of pixels on the LCoS. Maintaining the same absolute spectral resolution while increasing the spectral width requires a larger number of pixels, leading to a larger LCoS panel or higher numerical aperture optics that will increase the overall system's size and cost. Alternatively, if the spectral resolution is scaled with the total spectral width, such that the system maintains the same number of resolvable spectral channels, the WSSs will have essentially the same footprint and complexity. The increased use of superchannels, where multiple transponders are combined into a single band, indicates that the need to maintain the spectral resolution to efficiently route a single transponder may not be necessary. If the current network topology is retained, maintaining the same number of channels is sufficient to enable the same connectivity as today, but at a higher per link capacity.



## B. Amplification Technologies

Optical amplifiers were first used widely, instead of electronic repeaters, in optical transmission systems in the late 1990s, thanks to the invention of the EDFA. Although C-band (in particular) and L-band EDFAs have undergone constant improvement, particularly in terms of functionality, size, and cost, their spectral coverage has remained limited to approximately 40 nm in each band. Alternative rare-earth doped fiber amplifiers for the O-, E-, S- and U-bands have yet to be developed to sufficient maturity levels for widespread adoption in commercial transmission systems [83]. Therefore, although rare-earth-doped fibers based on thulium (S-band), neodymium (E-band), and praseodymium (O-band) have been demonstrated in numerous experiments and are also available commercially [84], and bismuth-doped fiber amplifiers offer potential amplification windows over various parts of the UWB spectrum considered here [85, 86], there remain practical manufacturing, handling, and reliability issues yet to be solved. Similarly, long-standing alternative optical amplification technologies based on semiconductor optical amplifiers [87] and optical parametric amplifiers [88, 89] have significant associated challenges in terms of either introducing nonlinear distortions, or with power efficiency and compactness, for them to be deployed in practice, despite a number of attractive features, including the recently demonstrated 100 nm bandwidth [87] and low NF plus supplementary functionality [89], respectively. In terms of spectral flexibility for UWB transmission, the Raman amplifier offers a potential short-term solution to amplification in most of the target UWB spectrum because, as explained in the following, it can provide an arbitrary gain bandwidth and the key components, high-power pump lasers, can be manufactured using existing, well-established techniques [83, 84].

Raman amplification in optical fiber is a long-standing all-optical amplification technology whose promise was widely explored in the 1990s and was commercially deployed in the early 2000s [16, 90]. However, its development slowed in the late 2000s, as explained in Section I, due to the rapid increases in spectral efficiency enabled by digital coherent transceivers [1]. Nevertheless, Raman amplifiers have found widespread commercial application over the years [52, 90, 91], both in long-distance, single-span, unrepeated transmissions, where distributed, or even multiple-order, Raman amplification provides improved NF [92], but also in conventional long-haul systems [90], where the long-standing, occasional use of hybrid EDFA/distributed Raman amplification technologies [93] has become much more common recently to support the higher OSNR requirements of advanced modulation formats [94]. In the context of UWB systems and networks, the highly flexible spectral characteristics of Raman amplifiers, which are mainly determined by the availability of suitably high-power pump lasers of appropriate wavelength, offer the potential for multi-band or even seamless UWB Raman amplification, either when deployed in their own right, or in concert with established C-band, or C+L-band EDFAs. In the following, we briefly review recent advances in the design and demonstration of a more complex class of UWB discrete Raman amplifiers, based

on a dual-stage design approach [95] and also recent achievements in the application of machine learning techniques to the design of multi-band Raman amplifiers. [96]. To increase the system OSNR, the so-called distributed Raman amplification is widely used, which in its simplest form comprises a number of high-power pumps multiplexed together and then coupled into the transmission fiber in a counter-propagating, or backward-pumped, configuration. However, to provide UWB gain, it is desirable to use a discrete, or lumped, Raman amplifier configuration, where all amplifier elements are located at the amplifier node [97]. Such a discrete Raman amplifier does not provide the NF benefits of distributed amplification, but it is functionally equivalent to a conventional EDFA. Moreover, it enables the use of a specialty nonlinear fiber as the Raman gain medium, leading to increased pump efficiency, and has the added safety benefit of not requiring a pump light in the operator's fiber plant.

## C. Mitigation of Transceiver Impairments

When it comes to the design of transceivers for UWB systems, there are, in principle, two design approaches: (1) design transceiver components specifically for UWB operation, i.e., covering several optical bands by a single device; and (2) design individual components optimized for operation over a single optical band. While option (1) will certainly simplify stock-keeping since a single transceiver type can cover all bands, option (2) will allow foreable better performance as transceivers only cover a single band, thus simplifying the optimized transceiver design. As outlined in Section III, transmitter and receiver components specifically developed for UWB operation, i.e., covering several optical bands by a single device, are still lacking. In particular, the following main components for optical UWB transceivers are not available as commercial products:

- UWB tunable laser
- UWB dual-polarization IQ modulator
- UWB coherent receiver frontend

First, the characterization of a UWB silicon photonics integrated transmitter and receiver showed that operation over 370 nm of bandwidth using a single device is, in principle, possible [98, 99]. However, since then, there was little to no progress reported (cf. overviews in [100, 101]). While specifically developed UWB transceiver components are widely unavailable, experimental investigation, in particular of S+C+L-band transmissions, currently relies mainly on C-band components, which are used out-of-band, coupled with digital mitigation schemes to cope with increased component-induced distortions. The following subsection provides an overview of recent works on transmitter components and the related DSP. Another option to cope with the unavailability of UWB components, which is based on optical signal processing and wavelength conversion, is presented in the next subsection.

In principle, silicon photonics modulators can provide UWB modulation due to the broadband nature of the plasma dispersion effect [98, 99, 101]. However, the only published results date back to 2016, and a comprehensive performance analysis is still lacking. In addition to silicon, lithium niobate

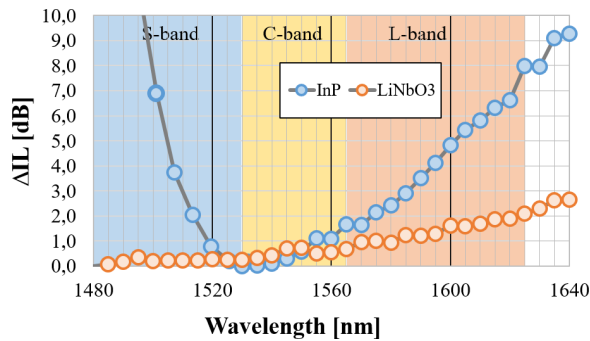


Fig. 9. Measured variation of insertion loss ( $\Delta IL$ ) of exemplary commercially available InP and LiNbO<sub>3</sub> C-band modulators in S-, C-, and L-band. In order to include wavelength dependency of modulation-induced loss, the measurements were performed under modulation conditions with 64 GBd dual-polarization 64-QAM signals.

(LiNbO<sub>3</sub>) and indium phosphide (InP) modulators are potential candidates for UWB modulation. Recently, a simulative study has evaluated several InP modulator designs [102]. One of the critical building blocks for UWB operation of InP is the integrated beam splitters usually implemented in the form of multi-mode interference (MMI) couplers. Due to the wavelength dependence of the MMI splitting ratio, their operation over a wide wavelength range can lead to significant variations in terms of insertion loss, power imbalance, and phase error of the modulator [103]. These variations can lead to unacceptable penalties [102]. However, initial results show that proper InP MMI designs can achieve a low variation of the splitting ratio and thus a high spectrum availability with low penalty [102]. An overview on the current state-of-the-art of UWB modulator devices is presented in a companion paper devoted to UWB devices in this special issue [78]. Here, we focus on the system aspects of UWB modulator operation. Due to the unavailability of UWB modulators, there have been efforts to use C-band modulators in UWB operation over the S-, C- and L-band and quantify their performance [104]. Depending on the material and design of the C-band modulators, there may be large differences in their suitability for out-of-band use. As an example, Fig. 9 shows the measured variation of insertion loss (IL) of two exemplary commercially-available dual-polarization I/Q modulators, one based on LiNbO<sub>3</sub> and the other on InP. The measurements consider the IL under modulation conditions (Dual-Polarization 64-QAM, symbol rate of 64 GBd, root-raised cosine pulse shape with 0.1 roll-off factor). In contrast to a CW measurement of the intrinsic IL, the modulation signal uses the full electro-optic bandwidth of the modulator. This way, the depicted variation of IL also includes the variation of the modulation-induced loss with wavelength. While the IL of the LiNbO<sub>3</sub> modulator is quite stable across the S+C+L-band, showing a variation of <2 dB, the InP modulator exhibits more than 10 dB variation. This has an important impact on the system performance, since the IL influences the maximum transmitter output power and thus the achievable GSNR (Eq. 1).

In addition to the individual components, DSP, which is performed at the transmitter and receiver sides, also needs to be adapted to UWB operation. For components operating over a wide wavelength range covering multiple bands, component

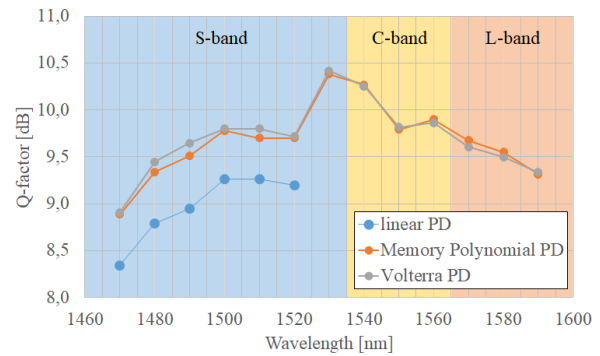


Fig. 10. Compensation of transmitter impairments by different digital pre-distortion techniques and per-wavelength autonomous optimization of filter design and coefficients (64-GBd DP-32QAM, LiNbO<sub>3</sub> DP-IQM).

specifications are expected to show a larger spread than only single-band conventional C-band operation. Advanced impairment estimation and compensation algorithms may help relax component specifications sufficiently to enable O- to L-band operation. In the past, there has already been various works focusing on the compensation of transmitter impairments in C-band by applying digital pre-distortion techniques. Such techniques play an important part in system design as they improve the achievable information rate of a system by removing limitations due to transmitter components [105]. Recently, an approach for autonomous nonlinear system identification and transmitter pre-distortion based on hyperparameter tuning by Bayesian optimization was proposed [106, 107]. The proposed scheme enables on-the-fly per-wavelength nonlinear system identification and pre-distortion of the whole transmitter subsystem including digital-to-analog converters, driver amplifiers, and modulators. The autonomous digital pre-distortion scheme was evaluated in an S+C+L-band transmission scenario [108]. Although a significant performance gain was achieved, the performance in the lower S-band is still degraded compared with the C-band as shown in Fig. 10, which displays the measured Q-factor in the S+C+L-band for linear and nonlinear pre-distortion either using a Volterra [109] or a reduced-complexity memory polynomial nonlinear [110] pre-distortion filter.

#### D. Whole Band Wavelength Conversion

As mentioned earlier in this paper, it is not necessarily straightforward to develop optical components that supports the full UWB spectrum. In particular, tunable lasers and optical amplifiers could be the most challenging components that should face certain limits of gain bandwidth defined by the material properties. Consequently, it becomes reasonable that the building blocks of a UWB network would start to use a mix of different types of devices, each of them covering a certain portion of the UWB spectrum (such as the one in Fig. 8 for instance). Such an architecture should also be beneficial from the viewpoint of initial investment to the line-system optics because the network can be constructed in a limited number of bands with a small initial investment, and incremental capacity enhancement can be achieved by introducing additional optical components for additional bands.

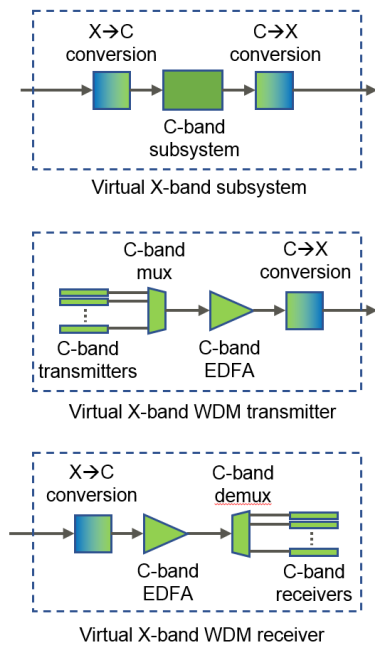


Fig. 11. Concept of new band subsystems based on C-band components and whole band wavelength conversion. Top: Virtual X-band in-line subsystem, Middle: Virtual X-band WDM transmitter, Bottom: Virtual X-band WDM receiver

However, this architecture still suffers from two issues: higher operational complexity and higher equipment cost. The operation complexity originates in the mixed use of different components that corresponds to different bands. Extra attention should be necessary during the network construction, upgrade, or reconstruction for similar-looking devices for different bands have to be connected to appropriate ports. Network operators should maintain a sufficient amount of inventory for possible upgrades or replacements for each component to cover different bands. Regarding the higher equipment cost, the new-band or UWB component should be limited in their production quantity, and thus the cost reduction should be more challenging compared with C-band components where the production volume should be larger. This cost issue should be critical, particularly with transceivers which are by far the largest in quantity among various network elements.

All-optical wavelength conversion technology that translates optical signals from one wavelength band to another can be considered as a solution to the aforementioned issues. As schematically shown in Fig. 11, a virtual subsystem for a new band (i.e. X-band) can be realized by inserting whole band wavelength converter(s) at the optical input and/or output port(s) of an existing C-band subsystem. This idea should be most effective when it is applied to the WDM transceivers because one converter can translate the whole WDM spectrum in the C-band to the X-band or vice versa altogether.

Among numerous wavelength conversion techniques reported in the past [111], the whole band wavelength converter to be used here is required to be inherently transparent to the signal: being agnostic to the number of channels in the WDM signal, symbol rate, and modulation format of each channel and signal polarization including the compatibility of

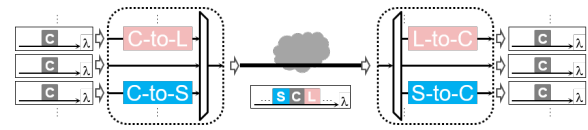


Fig. 12. Schematic of UWB transmission system using whole band wavelength conversion. Tx: Transceiver

polarization multiplexing. As a candidate to satisfy such requirements, highly nonlinear fiber has been considered as one of the most promising media to generate wavelength-translated idler through FWM between the input WDM signal and continuous-wave pump light(s) at one or two wavelength(s) [112]. Collective wavelength conversion without modulation format and polarization sensitivity was demonstrated with a highly nonlinear fiber incorporated in the polarization diversity configuration [113]. Note that the fiber nonlinearity, which is usually a source of signal impairment in a fiber-optic transmission system, plays a key role to provide new network functionality. Two main basic parameters that characterize the performance of the whole band wavelength converter are conversion efficiency and conversion bandwidth.

More recently this technique was utilized to propose and demonstrate a UWB transmission system by adopting the concept depicted in Fig. 11 [74, 114]. The proposed system comprises, in addition to multiple sets of C-band WDM transceivers and a transmission line, a wavelength-band multiplexer/de-multiplexer and a pair of wavelength converters that enables the virtual use of C-band WDM transceivers as X-band transceiver. With this scheme, UWB WDM transmission systems can be developed without transceivers operating in new bands but C-band transceivers that are more mature and at the forefront of new development Fig. 12. An experimental demonstration of this system concept was given in a triple-band (S+C+L-band) with 200-Gb/s (34-GBd DP-16QAM) test signals in 50-GHz spacing. The C-band WDM signal was translated by a wavelength converter having the characteristics shown in Figs. 13 (a) and (b). They were then multiplexed with the other WDM signal in the C-band to generate a triple-band WDM signal. The signal quality after the 40-km standard SMF transmission was received by a real-time digital coherent receiver in the C-band after band de-multiplexing and wavelength conversion back into the C-band in the same configuration as that of the transmitter side (Figs. 13 (c) and (d)), where no bit error was observed after performing forward error correction on all 240 channels.

Whole band wavelength conversion can play other roles in future optical networks by providing advanced functionality. Such functionality can include amplification [115], multi-band protection and bidirectional transmission [116], and transmission performance improvement by equalizing the signal quality by wavelength-band switching within a multi-span transmission system [117].

Major characteristics that determines the performance of the whole band wavelength converter are conversion bandwidth and conversion efficiency. Regarding the conversion bandwidth, the key limiting factor is the phase matching among the input signal, pump light, and wavelength-converted idler across a wide wavelength range. The conversion bandwidth



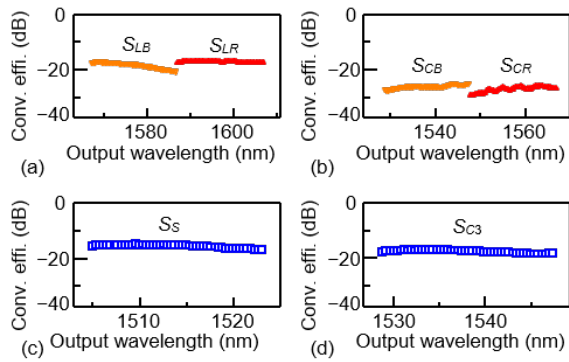


Fig. 13. Measured conversion efficiency of wavelength conversion for (a) C-to-L, (b) L-to-C, (c) C-to-S, and (d) S-to-C.

can be extended by using a shorter length of a nonlinear fiber [118], but group velocity tailoring of the nonlinear fiber [119] should be necessary to develop it with a practical pump light power of less than 1 W. Regarding the conversion efficiency, it is important to have a conversion with minimal loss across the wavelength band to avoid OSNR degradation in the network. Although the conversion efficiency is determined by the product of the nonlinear coefficient, the pump power, and the effective length of the nonlinear medium, its upper limit is capped by the saturation characteristics of the nonlinear medium. In wavelength conversion based on highly nonlinear fiber, stimulated Brillouin scattering (SBS) sets a limit to the pump power. The limitation imposed by SBS can be mitigated by broadening the spectral width of the pump light launched into the nonlinear fiber, and thus the conversion efficiency can be improved [120]. A potential problem in the coherent reception of the wavelength converted signal with the spectrally broadened pump light can be mitigated by a dual pump configuration with synchronous frequency dithering [121, 122], and can be considered to minimize such a penalty.

Further applications of wavelength conversion can be enabled by different types of nonlinear media in addition to the highly nonlinear fiber. One possible candidate should be a highly-efficient nonlinear medium that can provide a conversion gain such as periodically-poled lithium niobate waveguide [89]. The nonlinear waveguide using silicon-based semiconductor waveguide [123–125] is another interesting platform with a potential toward low power consumption and highly-functional integration in the future.

### E. Transmission in Hollow Core Fiber

As an alternative to SMF and solid-core fibers in general, HCFs were proposed in the 1990s [126]. However, for many years HCF loss remained very high and their usable optical bandwidth appeared to be relatively limited. The situation changed with the advent of HCFs of the NANF type, proposed in [25] in 2014. While the first fabricated NANFs still had high loss, steadily decreasing loss values were obtained in the following years. In 2019, the 1 dB/km mark was broken and recently a value of 0.174 dB/km over the C-band [26] has been reported. The results in [26] also indicate that, if the water peak was eliminated, the loss could be less than 0.23

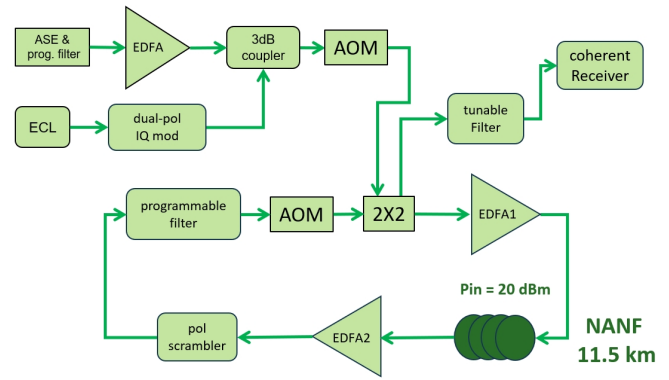


Fig. 14. Schematic of the NANF re-circulating loop experiment [128].

dB/km over 300+ nm and less than 0.3 dB/km over 400+ nm. Further improvement appears possible, too.

In addition to the low loss and large bandwidth, NANF also enjoys a Kerr nonlinearity coefficient  $\gamma$ , which is 3 to 4 orders of magnitude lower than SMF, due to the propagation in NANF occurring in gas. This means that both NLI and SRS are practically negligible in NANF, which behaves essentially as a linear medium. Another positive aspect of NANF is that the dispersion is low, about 2.5 ps/(nm · km). This could substantially ease the DSP effort for chromatic dispersion compensation, especially at the ultra-high symbol rates that are currently being developed. Another advantage of NANF is that light propagates at almost vacuum speed. The reduction of propagation time is attractive for certain applications where latency is important.

One critical aspect of NANF is inter-modal interference (IMI), which may occur because NANFs are intrinsically multimodal and achieve single-mode operation thanks to higher-order modes having large attenuation. If this mechanism of mode suppression is not effective, then substantial IMI can be present, which may cause significant transmission penalty. The threshold for negligible impact of IMI is estimated to be about -60 dB/km [127]. To test the behavior of NANFs in actual long-haul transmission, various re-circulating loop experiments have been carried out. The longest-reaching [128] involved a transmission of 41 PM-QPSK channels over 4,000 km of NANF at an average per-channel generalized mutual information (GMI) of 3.54 bit/symbol.

A variant of the experiment characterized each individual channel maximum reach (with all others still being transmitted). Maximum reach was defined as the maximum distance for which the channel GMI was  $\geq 3.5$  bit/symbol. Fig. 14 shows the schematic of the experiment. The results are shown in Fig. 15. Remarkably, some channels approached 6,000 km, which corresponds to over 500 turns in the re-circulating loop. Several exceeded 5,000 km. On the other hand, a few channels reached only about 3,000 km. This discrepancy in results was partly explained by dis-uniformity in spectral response of the loop at the hundreds of re-circulations which were being used, beyond the capability of the loop programmable filter resolution to cope with. Partly, it was attributed to non-negligible IMI, which was estimated to be about -50 dB/km. This value was confirmed by an independent direct measurement of the



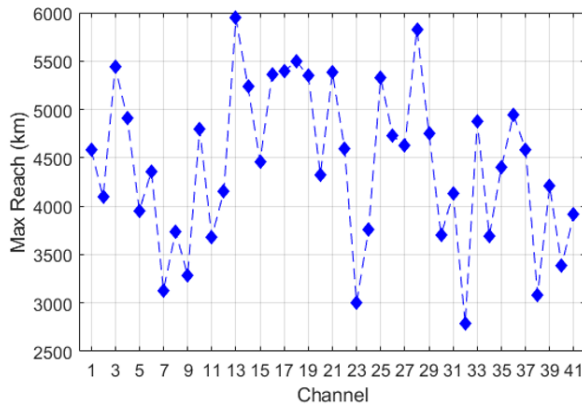


Fig. 15. Maximum reach of each individual channel of the experiment [128] whose schematic is shown in Fig. 14. Transmission was PM-QPSK at 32 GBd.

NANF, carried out by means of a sliding window and Fourier filtering analysis of the transmission spectrum [129].

The experiment [128] showed very significant progress vs. previous experiments, proving that NANF was on a quick development trend. This trend was confirmed by the latest specimen, presented in [26], which far outperforms the NANF used in [128]: loss is now below 0.2 dB/km, vs. 0.8 dB/km. In addition, the IMI of the NANF [26] has been measured to be between  $-54$  and  $-58$  dB/km, hence very close to the  $-60$  dB/km required for virtually no IMI impact. It can therefore be expected that when the latest generation NANF is tested in a long-haul experiment, better results and better uniformity among channels than [128] could be found. It should also be noted that an important condition for NANF to deliver new record long-haul performance is that longer stretches of fiber can be fabricated, than previously done. Performing re-circulating loop experiments over only a few km of fiber clearly makes experimentation difficult and introduces substantial set-up related spurious effects.

The potential of future NANFs to deliver a possibly larger throughput than SMF was theoretically investigated in [127]. It was found that, over 1,000 km links ( $10 \times 100$  km), NANF could deliver up to  $5 \times$ – $6 \times$  the throughput of a Raman-amplified (with 0 dB noise figure) SMF C+L system, assuming a NANF 0.2 dB/km loss across 400 nm of bandwidth and lumped amplification with a noise figure of 9 dB. Note that realizing such systems would require exceptional progress in many aspects: cost-effective top-performance NANF fabrication in quantity; suitable optical amplification and optical sources across hundreds of nm; development of many ancillary technologies needed for practical deployment. These are very substantial challenges. Nonetheless, the peculiar features of NANF are quite attractive and might make it a possible future contender for UWB systems.

## V. CONCLUSION

The fiber capacity increases that have been achieved over the last three decades have resulted primarily from increasing the spectral efficiency while using the same amplifier bandwidth. However, we are approaching the nonlinear Shannon limit, and this approach to scaling capacity is being rapidly exhausted.

Future system scaling will come through provisioning more bandwidth either in the form of a wider spectrum on a single fiber as discussed here or through copies of the existing spectrum on multiple spatial channels, as described in other papers in this issue. Given the diversity of locations and constraints on optical fiber systems, both approaches will likely be applicable in future networks. Extension of the optical bandwidth beyond the C+L-band is, therefore, expected to play a significant role in upgrading the capacity of future optical networks.

In this paper, we have considered the merits and challenges of a UWB optical transport system beyond conventional bands to meet this expected capacity growth. We have identified technologies and application areas where UWB may have a significant impact. We reviewed the state-of-the-art UWB system demonstrations, their enabling technologies, and unique technical issues to UWB systems such as system modeling and design, transceiver impairments, and optical amplification technologies. We also looked at a new type of fiber, hollow-core NANF, which might provide in the future ultra-wide bandwidths with negligible non-linearity. Furthermore, using whole band wavelength conversion was reviewed as a potential means to overcome cost-related challenges in the UWB network. This has the potential to allow the reuse of current conventional band components which would overcome the time and costs required to develop transmit and receive components for all the new bands.

## REFERENCES

- [1] P. J. Winzer, D. T. Neilson, and A. R. Chraplyvy, "Fiber-optic transmission and networking: The previous 20 and the next 20 years (invited)," *Opt. Exp.*, vol. 26, no. 18, pp. 24 190–24 239, Sep. 2018. DOI: [10.1364/OE.26.024190](https://doi.org/10.1364/OE.26.024190).
- [2] R. J. Mears, L. Reekie, I. M. Jauncey, and D. N. Payne, "Low-noise erbium-doped fibre amplifier operating at  $1.54 \mu\text{m}$ ," *Electron. Lett.*, vol. 23, no. 19, pp. 1026–1028, Sep. 1987. DOI: [10.1049/el:19870719](https://doi.org/10.1049/el:19870719).
- [3] E. Desurvire, J. R. Simpson, and P. C. Becker, "High-gain erbium-doped traveling-wave fiber amplifier," *Opt. Lett.*, vol. 12, no. 11, pp. 888–890, Nov. 1987. DOI: [10.1364/OL.12.000888](https://doi.org/10.1364/OL.12.000888).
- [4] M. Nakazawa, Y. Kimura, and K. Suzuki, "Efficient  $\text{Er}^{3+}$ -doped optical fiber amplifier pumped by a  $1.48 \mu\text{m}$  InGaAsP laser diode," *Appl. Phys. Lett.*, vol. 54, no. 4, pp. 295–297, Jan. 1989. DOI: [10.1063/1.101448](https://doi.org/10.1063/1.101448).
- [5] *Transmission systems and media, digital systems and networks*, ITU-T G.Sup39, Feb. 2016.
- [6] M. Jinno, T. Sakamoto, J. Kani, S. Aisawa, K. Oda, M. Fukui, H. Ono, and K. Oguchi, "First demonstration of 1580 nm wavelength band WDM transmission for doubling usable bandwidth and suppressing FWM in DSF," *Electron. Lett.*, vol. 33, no. 10, pp. 882–883, May 1997. DOI: [10.1049/el:19970584](https://doi.org/10.1049/el:19970584).

- [7] Y. Sun, J. W. Sulhoff, A. K. Srivastava, J. L. Zyskind, C. Wolf, T. A. Strasser, J. R. Pedrazzani, J. B. Judkins, R. P. Espindola, A. M. Vengsardar, and J. Zhou, "An 80 nm ultra wide band EDFA with low noise figure and high output power," in *Proc. 23rd Eur. Conf. Opt. Commun.*, vol. 5, 1997, 69–72 vol.5. DOI: [10.1049/cp:19971614](https://doi.org/10.1049/cp:19971614).
- [8] J. F. Massicot, J. R. Armitage, R. Wyatt, B. J. Ainslie, and S. P. Craig-Ryan, "High gain, broadband, 1.6  $\mu\text{m}$   $\text{Er}^{3+}$  doped silica fibre amplifier," *Electron. Lett.*, vol. 26, no. 20, pp. 1645–1646, Sep. 1990. DOI: [10.1049/el:19901053](https://doi.org/10.1049/el:19901053).
- [9] H. Ono, M. Yamada, and Y. Ohishi, "Gain-flattened  $\text{Er}^{3+}$ -doped fiber amplifier for a WDM signal in the 1.57–1.60- $\mu\text{m}$  wavelength region," *IEEE Photon. Technol. Lett.*, vol. 9, no. 5, pp. 596–598, May 1997. DOI: [10.1109/68.588134](https://doi.org/10.1109/68.588134).
- [10] J. Kani, K. Hattori, M. Jinno, T. Kanamori, and K. Oguchi, "Triple-wavelength-band WDM transmission over cascaded dispersion-shifted fibers," *IEEE Photon. Technol. Lett.*, vol. 11, no. 11, pp. 1506–1508, Nov. 1999. DOI: [10.1109/68.803094](https://doi.org/10.1109/68.803094).
- [11] E. Ishikawa, M. Nishihara, Y. Sato, C. Ohshima, Y. Sugaya, and J. Kumasako, "Novel 1500 nm-band EDFA with discrete Raman amplifier," in *Proc. 27th Eur. Conf. Opt. Commun.*, 2001, 48–49 vol.6. DOI: [10.1109/ECOC.2001.989043](https://doi.org/10.1109/ECOC.2001.989043).
- [12] K. Fukuchi, T. Kasamatsu, M. Morie, R. Ohhira, T. Ito, K. Sekiya, D. Ogasahara, and T. Ono, "10.92-Tb/s (273  $\times$  40-Gb/s) triple-band/ultra-dense WDM optical-repeated transmission experiment," in *Proc. Opt. Fiber Commun. Conf.*, 2001, PD24. DOI: [10.1364/OFC.2001.PD24](https://doi.org/10.1364/OFC.2001.PD24).
- [13] T. Tanaka, K. Torii, M. Yuki, H. Nakamoto, T. Naito, and I. Yokota, "200-nm bandwidth WDM transmission around 1.55  $\mu\text{m}$  using distributed Raman amplifier," in *Proc. 28th Eur. Conf. Opt. Commun.*, vol. 5, 2002, PD4.6.
- [14] C. E. Shannon, "A mathematical theory of communication," *The Bell System Technical Journal*, vol. 27, no. 3, pp. 379–423, Jul. 1948. DOI: [10.1002/j.1538-7305.1948.tb01338.x](https://doi.org/10.1002/j.1538-7305.1948.tb01338.x).
- [15] X. Liu, "Evolution of fiber-optic transmission and networking toward the 5G era," *iScience*, vol. 22, pp. 489–506, Dec. 2019. DOI: [10.1016/j.isci.2019.11.026](https://doi.org/10.1016/j.isci.2019.11.026).
- [16] D. A. Fishman, W. A. Thompson, and L. Vallone, "LambdaXtreme® transport system: R&D of a high capacity system for low cost, ultra long haul DWDM transport," *Bell Labs Technical Journal*, vol. 11, no. 2, pp. 27–53, 2006. DOI: [10.1002/bltj.20160](https://doi.org/10.1002/bltj.20160).
- [17] V. Vusirikala, X. Zhao, T. Hofmeister, V. Kamalov, V. Dangui, and B. Koley, "Scalable and flexible transport networks for inter-datacenter connectivity," in *Proc. Opt. Fiber Commun. Conf.*, 2015, Tu3H.1. DOI: [10.1364/OFC.2015.Tu3H.1](https://doi.org/10.1364/OFC.2015.Tu3H.1).
- [18] M. Cantono, R. Schmogrow, M. Newland, V. Vusirikala, and T. Hofmeister, "Opportunities and challenges of C+L transmission systems," *J. Lightw. Technol.*, vol. 38, no. 5, pp. 1050–1060, Mar. 2020. DOI: [10.1109/JLT.2019.2959272](https://doi.org/10.1109/JLT.2019.2959272).
- [19] A. Ferrari, A. Napoli, J. Fischer, N. Costa, A. D'amico, J. Pedro, W. Forysiak, E. Pincemin, A. Lord, A. Stavdas, J. Fernandez-palacios Gimenez, G. Roelkens, N. Calabretta, S. Abrate, B. Sommerkorn-krombholz, and V. Curri, "Assessment on the achievable throughput of multi-band ITU-T G.652.D fiber transmission systems," *J. Lightw. Technol.*, vol. 38, no. 16, pp. 4279–4291, Aug. 2020. DOI: [10.1109/JLT.2020.2989620](https://doi.org/10.1109/JLT.2020.2989620).
- [20] G. Agrawal, *Nonlinear Fiber Optics*. Elsevier, 2007. DOI: [10.1007/3-540-46629-0\\_9](https://doi.org/10.1007/3-540-46629-0_9).
- [21] D. Marcuse, A. Chraplyvy, and R. Tkach, "Dependence of cross-phase modulation on channel number in fiber WDM systems," *J. Lightw. Technol.*, vol. 12, no. 5, pp. 885–890, Mar. 1994. DOI: [10.1109/50.293982](https://doi.org/10.1109/50.293982).
- [22] R.-J. Essiambre, G. Kramer, P. J. Winzer, G. J. Foschini, and B. Goebel, "Capacity limits of optical fiber networks," *J. Lightw. Technol.*, vol. 28, no. 4, pp. 662–701, Feb. 2010. DOI: [10.1109/JLT.2009.2039464](https://doi.org/10.1109/JLT.2009.2039464).
- [23] R. H. Stolen, E. P. Ippen, and A. R. Tynes, "Raman oscillation in glass optical waveguide," *Appl. Phys. Lett.*, vol. 20, no. 2, pp. 62–64, Jan. 1972. DOI: [10.1063/1.1654046](https://doi.org/10.1063/1.1654046).
- [24] H. Kidorf, K. Rottwitt, M. Nissov, M. Ma, and E. Rabarjaona, "Pump interactions in a 100-nm bandwidth Raman amplifier," *IEEE Photon. Technol. Lett.*, vol. 11, no. 5, pp. 530–532, May 1999. DOI: [10.1109/68.759388](https://doi.org/10.1109/68.759388).
- [25] F. Poletti, "Nested antiresonant nodeless hollow core fiber," *Opt. Exp.*, vol. 22, no. 20, pp. 23 807–23 828, Sep. 2014. DOI: [10.1364/OE.22.023807](https://doi.org/10.1364/OE.22.023807).
- [26] G. T. Jasion, H. Sakr, J. R. Hayes, S. R. Sandoghchi, L. Hooper, E. N. Fokoua, A. Saljoghei, H. C. Mulvad, M. Alonso, A. Tarantam, T. D. Bradley, I. A. Davidson, Y. Chen, D. J. Richardson, and F. Poletti, "0.174 dB/km hollow core double nested antiresonant nodeless fiber (DNANF)," in *Proc. Opt. Fiber Commun. Conf. (OFC)*, 2022, Th4.C.7.
- [27] A. Mecozzi and R.-J. Essiambre, "Nonlinear Shannon limit in pseudolinear coherent systems," *J. Lightw. Technol.*, vol. 30, no. 12, pp. 2011–2024, Jun. 2012. DOI: [10.1109/JLT.2012.2190582](https://doi.org/10.1109/JLT.2012.2190582).
- [28] R. Dar, M. Feder, A. Mecozzi, and M. Shtaif, "Properties of nonlinear noise in long, dispersion-uncompensated fiber links," *Opt. Exp.*, vol. 21, no. 22, pp. 25 685–25 699, Nov. 2013. DOI: [10.1364/OE.21.025685](https://doi.org/10.1364/OE.21.025685).
- [29] P. Poggiolini, G. Bosco, A. Carena, V. Curri, Y. Jiang, and F. Forghieri, "The GN-model of fiber non-linear propagation and its applications," *J. Lightw. Technol.*, vol. 32, no. 4, pp. 694–721, Feb. 2014. DOI: [10.1109/JLT.2013.2295208](https://doi.org/10.1109/JLT.2013.2295208).
- [30] A. Carena, G. Bosco, V. Curri, Y. Jiang, P. Poggiolini, and F. Forghieri, "EGN model of non-linear fiber prop-

- agation,” *Opt. Exp.*, vol. 22, no. 13, pp. 16 335–16 362, Jun. 2014. DOI: [10.1364/OE.22.016335](https://doi.org/10.1364/OE.22.016335).
- [31] R. Dar, M. Feder, A. Mecozzi, and M. Shttaif, “Accumulation of nonlinear interference noise in fiber-optic systems,” *Opt. Exp.*, vol. 22, no. 12, pp. 14 199–14 211, Jun. 2014. DOI: [10.1364/OE.22.014199](https://doi.org/10.1364/OE.22.014199).
- [32] V. Curri, “Software-defined WDM optical transport in disaggregated open optical networks,” in *Proc. 22nd Int. Conf. Transparent Opt. Netw.*, 2020, pp. 1–4. DOI: [10.1109/ICTON51198.2020.9203450](https://doi.org/10.1109/ICTON51198.2020.9203450).
- [33] A. Bononi, O. Beucher, and P. Serena, “Single- and cross-channel nonlinear interference in the Gaussian noise model with rectangular spectra,” *Opt. Exp.*, vol. 21, no. 26, pp. 32 254–32 268, Dec. 2013. DOI: [10.1364/OE.21.032254](https://doi.org/10.1364/OE.21.032254).
- [34] M. Filer, M. Cantono, A. Ferrari, G. Grammel, G. Galimberti, and V. Curri, “Multi-vendor experimental validation of an open source QoT estimator for optical networks,” *J. Lightw. Technol.*, vol. 36, no. 15, pp. 3073–3082, Aug. 2018. DOI: [10.1109/JLT.2018.2818406](https://doi.org/10.1109/JLT.2018.2818406).
- [35] A. Pilipetskii, D. Kovsh, E. Mateo, E. R. Hartling, G. Mohs, L. Jovanovski, M. Salsi, M. Cantono, M. Bolshtyansky, O. Courtois, O. Gautheron, O. A. Sab, P. Pecci, P. Mehta, S. Grubb, T. Inoue, V. Kamalov, V. Vusirikala, V. Letellier, and Y. Inada, “The subsea fiber as a Shannon channel,” in *Proc. SubOptic 2019*, 2019.
- [36] A. Ferrari, M. Filer, K. Balasubramanian, Y. Yin, E. L. Rouzic, J. Kundrát, G. Grammel, G. Galimberti, and V. Curri, “GNPy: An open source application for physical layer aware open optical networks,” *J. Opt. Commun. Netw.*, vol. 12, no. 6, pp. C31–C40, Jun. 2020. DOI: [10.1364/JOCN.382906](https://doi.org/10.1364/JOCN.382906).
- [37] V. Curri, A. Carena, A. Arduino, G. Bosco, P. Poggiolini, A. Nespola, and F. Forghieri, “Design strategies and merit of system parameters for uniform uncompensated links supporting Nyquist-WDM transmission,” *J. Lightw. Technol.*, vol. 33, no. 18, pp. 3921–3932, Sep. 2015. DOI: [10.1109/JLT.2015.2447151](https://doi.org/10.1109/JLT.2015.2447151).
- [38] A. D’Amico, E. London, B. Le Guyader, F. Frank, E. Le Rouzic, E. Pincemin, N. Brochier, and V. Curri, “GNPy experimental validation on flex-grid, flex-rate WDM optical transport scenarios,” in *Proc. Opt. Fiber Commun. Conf.*, 2021, W1G.2.
- [39] H. Sun, M. Torbatian, M. Karimi, R. Maher, S. Thomson, M. Tehrani, Y. Gao, A. Kumpera, G. Soliman, A. Kakkar, M. Osman, Z. A. El-Sahn, C. Doggart, W. Hou, S. Sutarwala, Y. Wu, M. R. Chitgarha, V. Lal, H.-S. Tsai, S. Corzine, J. Zhang, J. Osenbach, S. Buggaveeti, Z. Morbi, M. I. Olmedo, I. Leung, X. Xu, P. Samra, V. Dominic, S. Sanders, M. Ziari, A. Napoli, B. Spinnler, K.-T. Wu, and P. Kandappan, “800G DSP ASIC design using probabilistic shaping and digital sub-carrier multiplexing,” *J. Lightw. Technol.*, vol. 38, no. 17, pp. 4744–4756, Sep. 2020. DOI: [10.1364/JLT.38.004744](https://doi.org/10.1364/JLT.38.004744).
- [40] F. P. Guiomar, R. Li, C. R. S. Fludger, A. Carena, and V. Curri, “Hybrid modulation formats enabling elastic fixed-grid optical networks,” *J. Opt. Commun. Netw.*, vol. 8, no. 7, A92–A100, Jul. 2016. DOI: [10.1364/JOCN.8.000A92](https://doi.org/10.1364/JOCN.8.000A92).
- [41] J. Cho and P. J. Winzer, “Probabilistic constellation shaping for optical fiber communications,” *J. Lightw. Technol.*, vol. 37, no. 6, pp. 1590–1607, Mar. 2019. DOI: [10.1109/JLT.2019.2898855](https://doi.org/10.1109/JLT.2019.2898855).
- [42] V. Curri and A. Carena, “Merit of Raman pumping in uniform and uncompensated links supporting NyWDM transmission,” *J. Lightw. Technol.*, vol. 34, no. 2, pp. 554–565, Jan. 2016. DOI: [10.1109/JLT.2015.2477599](https://doi.org/10.1109/JLT.2015.2477599).
- [43] E. Ip and J. M. Kahn, “Compensation of dispersion and nonlinear impairments using digital backpropagation,” *J. Lightw. Technol.*, vol. 26, no. 20, pp. 3416–3425, Oct. 2008. DOI: [10.1109/JLT.2008.927791](https://doi.org/10.1109/JLT.2008.927791).
- [44] D. Marcuse, C. R. Manyuk, and P. K. A. Wai, “Application of the Manakov-PMD equation to studies of signal propagation in optical fibers with randomly varying birefringence,” *J. Lightw. Technol.*, vol. 15, no. 9, pp. 1735–1746, Sep. 1997. DOI: [10.1109/50.622902](https://doi.org/10.1109/50.622902).
- [45] J. E. Aber, M. C. Newstein, and B. A. Garetz, “Femtosecond optical Kerr effect measurements in silicate glasses,” *J. Opt. Soc. Am. B*, vol. 17, no. 1, pp. 120–127, Jan. 2000. DOI: [10.1364/JOSAB.17.000120](https://doi.org/10.1364/JOSAB.17.000120).
- [46] S. Walker, “Rapid modeling and estimation of total spectral loss in optical fibers,” *J. Lightw. Technol.*, vol. 4, no. 8, pp. 1125–1131, Aug. 1986. DOI: [10.1109/JLT.1986.1074874](https://doi.org/10.1109/JLT.1986.1074874).
- [47] G. Borracini, A. D’Amico, S. Straullu, A. Nespola, S. Piciaccia, A. Tanzi, G. Galimberti, S. Bottacchi, S. Swail, and V. Curri, “Cognitive and autonomous QoT-driven optical line controller,” *J. Opt. Commun. Netw.*, vol. 13, no. 10, E23–E31, Oct. 2021. DOI: [10.1364/JOCN.424021](https://doi.org/10.1364/JOCN.424021).
- [48] C. R. S. Fludger, V. Handerek, and R. J. Mears, “Pump to signal RIN transfer in Raman fiber amplifiers,” *J. Lightw. Technol.*, vol. 19, no. 8, p. 1140, Aug. 2001. DOI: [10.1109/50.939794](https://doi.org/10.1109/50.939794).
- [49] K. Rottwitt, J. Bromage, A. J. Stentz, L. Leng, M. E. Lines, and H. Smith, “Scaling of the Raman gain coefficient: Applications to germanosilicate fibers,” *J. Lightw. Technol.*, vol. 21, no. 7, p. 1652, Jul. 2003. DOI: [10.1109/JLT.2003.814386](https://doi.org/10.1109/JLT.2003.814386).
- [50] N. Sambo, A. Ferrari, A. Napoli, J. Pedro, L. S. Kiani, P. Castoldi, and V. Curri, “Multiband seamless network upgrade by exploiting the e-band,” in *2021 European Conference on Optical Communication (ECOC)*, 2021, pp. 1–4. DOI: [10.1109/ECOC52684.2021.9606095](https://doi.org/10.1109/ECOC52684.2021.9606095).
- [51] F. Vanholsbeeck, S. Coen, P. Emplit, M. Haelterman, and T. Sylvestre, “Raman-induced power tilt in arbitrarily large wavelength-division-multiplexed systems,” *IEEE Photon. Technol. Lett.*, vol. 17, no. 1, pp. 88–90, Jan. 2005. DOI: [10.1109/LPT.2004.837726](https://doi.org/10.1109/LPT.2004.837726).



- [52] J. Bromage, "Raman amplification for fiber communications systems," *J. Lightw. Technol.*, vol. 22, no. 1, p. 79, Jan. 2004. DOI: [10.1109/JLT.2003.822828](https://doi.org/10.1109/JLT.2003.822828).
- [53] M. Cantono, D. Pileri, A. Ferrari, C. Catanese, J. Thouras, J.-L. Augé, and V. Curri, "On the interplay of nonlinear interference generation with stimulated Raman scattering for QoT estimation," *J. Lightw. Technol.*, vol. 36, no. 15, pp. 3131–3141, Aug. 2018. DOI: [10.1109/JLT.2018.2814840](https://doi.org/10.1109/JLT.2018.2814840).
- [54] D. Semrau, R. I. Killey, and P. Bayvel, "The Gaussian noise model in the presence of inter-channel stimulated Raman scattering," *J. Lightw. Technol.*, vol. 36, no. 14, pp. 3046–3055, Jul. 2018. DOI: [10.1109/JLT.2018.2830973](https://doi.org/10.1109/JLT.2018.2830973).
- [55] B. Correia, R. Sadeghi, E. Virgillito, A. Napoli, N. Costa, J. Pedro, and V. Curri, "Power control strategies and network performance assessment for C+L+S multiband optical transport," *J. Opt. Commun. Netw.*, vol. 13, no. 7, pp. 147–157, Jul. 2021. DOI: [10.1364/JOCN.419293](https://doi.org/10.1364/JOCN.419293).
- [56] V. Oliari, E. Agrell, and A. Alvarado, "Regular perturbation on the group-velocity dispersion parameter for nonlinear fibre-optical communications," *Nature Commun.*, vol. 11, no. 1, Feb. 2020. DOI: [10.1038/s41467-020-14503-w](https://doi.org/10.1038/s41467-020-14503-w).
- [57] M. Eiselt, R. M. Jopson, and R. H. Stolen, "Nondestructive position-resolved measurement of the zero-dispersion wavelength in an optical fiber," *J. Lightw. Technol.*, vol. 15, no. 1, pp. 135–143, Jan. 1997. DOI: [10.1109/50.552121](https://doi.org/10.1109/50.552121).
- [58] B. J. Puttnam, R. S. Luís, G. Rademacher, M. Mendez-Astudilio, Y. Awaji, and H. Furukawa, "S, C and extended L-band transmission with doped fiber and distributed Raman amplification," in *Proc. Opt. Fiber Commun. Conf.*, 2021, Th4C.2.
- [59] L. Galdino, A. Edwards, W. Yi, E. Sillescu, Y. Wakayama, T. Gerard, W. S. Pelouch, S. Barnes, T. Tsuritani, R. I. Killey, D. Lavery, and P. Bayvel, "Optical fibre capacity optimisation via continuous bandwidth amplification and geometric shaping," *IEEE Photon. Technol. Lett.*, vol. 32, no. 17, pp. 1021–1024, Sep. 2020. DOI: [10.1109/LPT.2020.3007591](https://doi.org/10.1109/LPT.2020.3007591).
- [60] F. Hamaoka, K. Minoguchi, T. Sasai, A. Matsushita, M. Nakamura, S. Okamoto, E. Yamazaki, and Y. Kisaka, "150.3-Tb/s ultra-wideband (S, C, and L bands) single-mode fibre transmission over 40-km using >519Gb/s/A PDM-128QAM signals," in *Proc. 44th Eur. Conf. Opt. Commun.*, 2018, Mo4G.1. DOI: [10.1109/ECOC.2018.8535140](https://doi.org/10.1109/ECOC.2018.8535140).
- [61] J. Renaudier, A. C. Meseguer, A. Ghazisaeidi, P. Tran, R. R. Muller, R. Brenot, A. Verdier, F. Blache, K. Mekhazni, B. Duval, H. Debregeas, M. Achouche, A. Boutin, F. Morin, L. Letteron, N. Fontaine, Y. Frignac, and G. Charlet, "First 100-nm continuous-band WDM transmission system with 115Tb/s transport over 100km using novel ultra-wideband semiconductor optical amplifiers," in *Proc. 43rd Eur. Conf. Opt. Commun.*, 2017, Th.PDP.A.3. DOI: [10.1109/ECOC.2017.8346084](https://doi.org/10.1109/ECOC.2017.8346084).
- [62] A. Sano, T. Kobayashi, S. Yamanaka, A. Matsuura, H. Kawakami, Y. Miyamoto, K. Ishihara, and H. Masuda, "102.3-Tb/s (224 ×548-Gb/s) C- and extended L-band all-Raman transmission over 240 km using PDM-64QAM single carrier FDM with digital pilot tone," in *Proc. Nat. Fiber Opt. Eng. Conf.*, 2012, PDP5C.3. DOI: [10.1364/NFOEC.2012.PDP5C.3](https://doi.org/10.1364/NFOEC.2012.PDP5C.3).
- [63] J. Renaudier, A. Arnould, D. Le Gac, A. Ghazisaeidi, P. Brindel, M. Makhisyian, A. Verdier, K. Mekhazni, F. Blache, H. Debregeas, A. Boutin, N. Fontaine, D. Neilson, R. Ryf, H. Chen, M. Achouche, and G. Charlet, "107 Tb/s transmission of 103-nm bandwidth over 3×100 km SSMF using ultra-wideband hybrid Raman/SOA repeaters," in *Proc. Opt. Fiber Commun. Conf.*, 2019, Tu3F.2. DOI: [10.1364/OFC.2019.Tu3F.2](https://doi.org/10.1364/OFC.2019.Tu3F.2).
- [64] L. Galdino, D. Semrau, M. Ionescu, A. Edwards, W. Pelouch, S. Desbruslais, J. James, E. Sillescu, D. Lavery, S. Barnes, R. I. Killey, and P. Bayvel, "Study on the impact of nonlinearity and noise on the performance of high-capacity broadband hybrid Raman-EDFA amplified system," *J. Lightw. Technol.*, vol. 37, no. 21, pp. 5507–5515, Nov. 2019. DOI: [10.1109/JLT.2019.2933246](https://doi.org/10.1109/JLT.2019.2933246).
- [65] J.-X. Cai, H. G. Batshon, M. V. Mazurczyk, C. R. Davidson, O. V. Sinkin, D. Wang, M. Paskov, W. W. Patterson, M. A. Bolshtyansky, and D. G. Foursa, "94.9 Tb/s single mode capacity demonstration over 1,900 km with C+L EDFAs and coded modulation," in *Proc. 44th Eur. Conf. Opt. Commun.*, 2018, Mo4G.3. DOI: [10.1109/ECOC.2018.8535554](https://doi.org/10.1109/ECOC.2018.8535554).
- [66] M. Ionescu, D. Lavery, A. Edwards, E. Sillescu, D. Semrau, L. Galdino, R. I. Killey, W. Pelouch, S. Barnes, and P. Bayvel, "74.38 Tb/s transmission over 6300 km single mode fibre enabled by C+L amplification and geometrically shaped PDM-64QAM," *J. Lightw. Technol.*, vol. 38, no. 2, pp. 531–537, Jan. 2020. DOI: [10.1109/JLT.2019.2954458](https://doi.org/10.1109/JLT.2019.2954458).
- [67] J.-X. Cai, H. G. Batshon, M. V. Mazurczyk, O. V. Sinkin, D. Wang, M. Paskov, W. W. Patterson, C. R. Davidson, P. C. Corbett, G. M. Wolter, T. E. Hammon, M. A. Bolshtyansky, D. G. Foursa, and A. N. Pilipetskii, "70.46 Tb/s over 7,600 km and 71.65 Tb/s over 6,970 km transmission in C+L band using coded modulation with hybrid constellation shaping and nonlinearity compensation," *J. Lightw. Technol.*, vol. 36, no. 1, pp. 114–121, Jan. 2018. DOI: [10.1109/JLT.2017.2757281](https://doi.org/10.1109/JLT.2017.2757281).
- [68] J.-X. Cai, Y. Sun, H. Zhang, H. G. Batshon, M. V. Mazurczyk, O. V. Sinkin, D. G. Foursa, and A. Pilipetskii, "49.3 Tb/s transmission over 9100 km using C+L EDFA and 54 Tb/s transmission over 9150 km using hybrid-Raman EDFA," *J. Lightw. Technol.*, vol. 33, no. 13, pp. 2724–2734, Jul. 2015. DOI: [10.1109/JLT.2015.2409846](https://doi.org/10.1109/JLT.2015.2409846).
- [69] J.-X. Cai, H. G. Batshon, M. V. Mazurczyk, O. V. Sinkin, D. Wang, M. Paskov, C. R. Davidson, W. W.



- Patterson, A. Turukhin, M. A. Bolshtyansky, and D. G. Foursa, "51.5 Tb/s capacity over 17,107 km in C+L bandwidth using single-mode fibers and nonlinearity compensation," *J. Lightw. Technol.*, vol. 36, no. 11, pp. 2135–2141, Jun. 2018. DOI: [10.1109/JLT.2018.2802322](https://doi.org/10.1109/JLT.2018.2802322).
- [70] A. Napoli, N. Calabretta, J. K. Fischer, N. Costa, S. Abrate, J. Pedro, V. Lopez, V. Curri, D. Zibar, E. Pincemin, S. Grot, G. Roelkens, C. Matrakidis, and W. Forysiak, "Perspectives of multi-band optical communication systems," in *Proc. 23rd Opto-Electron. and Commun. Conf.*, 2018, 5B3–1. DOI: [10.1109/OECC.2018.8730026](https://doi.org/10.1109/OECC.2018.8730026).
- [71] B. Puttnam, R. Luis, G. Rademacher, Y. Awaji, and H. Furukawa, "319 Tb/s transmission over 3001 km with S, C and L band signals over >120nm bandwidth in 125  $\mu$ m wide 4-core fiber," in *Proc. Opt. Fiber Commun. Conf.*, 2021, F3B.3.
- [72] J.-X. Cai, Y. Hu, A. Turukhin, M. V. Mazurczyk, M. Paskov, H. G. Batshon, C. R. Davidson, M. Bolshtyansky, and D. G. Foursa, "On the effects of transmitter induced channel correlation in broadband WDM transmission," in *Proc. Opt. Fiber Commun. Conf.*, 2018, Th1C.1. DOI: [10.1364/OFC.2018.Th1C.1](https://doi.org/10.1364/OFC.2018.Th1C.1).
- [73] D. J. Elson, G. Saavedra, K. Shi, D. Semrau, L. Galdino, R. Killey, B. C. Thomsen, and P. Bayvel, "Investigation of bandwidth loading in optical fibre transmission using amplified spontaneous emission noise," *Opt. Exp.*, vol. 25, no. 16, pp. 19 529–19 537, Aug. 2017. DOI: [10.1364/OE.25.019529](https://doi.org/10.1364/OE.25.019529).
- [74] T. Kato, S. Watanabe, T. Yamauchi, G. Nakagawa, H. Muranaka, Y. Tanaka, Y. Akiyama, and T. Hoshida, "Real-time transmission of 240×200-Gb/s signal in S+C+L triple-band wdm without S- or L-band transceivers," in *Proc. 45th Eur. Conf. Opt. Commun.*, 2019, PD1.7. DOI: [10.1049/cp.2019.1021](https://doi.org/10.1049/cp.2019.1021).
- [75] H. Buglia, E. Sillekens, A. Vasylenkova, P. Bayve, and L. Galdino, "On the impact of launch power optimisation and transceiver noise on the performance of ultra-wideband transmission systems," *J. Opt. Commun. Netw.*, vol. 14, no. 5, pp. 11–21, 2022. DOI: [10.1364/JOCN.450726](https://doi.org/10.1364/JOCN.450726).
- [76] J.-X. Cai, G. Mohs, and N. S. Bergano, "Chapter 13 - ultralong-distance undersea transmission systems," in *Optical Fiber Telecommunications VII*, A. E. Willner, Ed., Academic Press, 2020, pp. 565–625. DOI: [10.1016/B978-0-12-816502-7.00015-4](https://doi.org/10.1016/B978-0-12-816502-7.00015-4).
- [77] P. Trischitta, M. Colas, M. Green, G. Wuzniak, and J. Arena, "The TAT-12/13 cable network," *IEEE Commun. Mag.*, vol. 34, no. 2, pp. 24–28, Feb. 1996. DOI: [10.1109/35.481240](https://doi.org/10.1109/35.481240).
- [78] J. Renaudier, A. Napoli, M. Ionescu, C. Calo, G. Fiol, V. Mikhailov, N. Fontaine, F. Poletti, and P. Poggiolini, "Devices and components for ultra-wideband optical communications," *Proceedings of the IEEE*, 2022, to be published.
- [79] B. C. Collings, "Advanced ROADM technologies and architectures," in *Proc. Opt. Fiber Commun. Conf.*, 2015, Tu3D.3. DOI: [10.1364/OFC.2015.Tu3D.3](https://doi.org/10.1364/OFC.2015.Tu3D.3).
- [80] H. Chen, N. K. Fontaine, B. Huang, X. Xiao, R. Ryf, and D. T. Neilson, "Wavelength selective switch for dynamic VCSEL-based data centers," in *Proc. 42nd Eur. Conf. Opt. Commun.*, 2016, Th.3.B.1.
- [81] N. K. Fontaine, M. Mazur, R. Ryf, H. Chen, L. Dallachiesa, and D. T. Neilson, "36-THz bandwidth wavelength selective switch," in *Proc. 47th Eur. Conf. Opt. Commun.*, 2021, Th3C1–PD2.3. DOI: [10.1109/ECOC52684.2021.9606114](https://doi.org/10.1109/ECOC52684.2021.9606114).
- [82] Lightwave, Ed., *Finisar WSS: Flexgrid(R) C+L wavelength selective switch*, [Online; archived 9-July-2021], Mar. 2021. [Online]. Available: <https://web.archive.org/web/20210709135938/https://www.lightwaveonline.com/test/design-manufacturing/article/14199805/finisar-wss-flexgrid-cl-wavelength-selective-switch>.
- [83] L. Rapp and M. Eiselt, "Optical amplifiers for wide-band optical transmission systems," in *Proc. Opt. Fiber Commun. Conf.*, 2021, Th4C.1.
- [84] —, "Ultra-wideband amplification strategies," in *Proc. IEEE Photonics Society Summer Topicals Meeting Series*, 2021, pp. 1–2. DOI: [10.1109/SUM48717.2021.9505858](https://doi.org/10.1109/SUM48717.2021.9505858).
- [85] A. Donodin, V. Dvoyrin, E. Manuylovich, L. Krzaczanowicz, W. Forysiak, M. Melkumov, V. Mashinsky, and S. Turitsyn, "Bismuth doped fibre amplifier operating in E- and S- optical bands," *Opt. Mater. Exp.*, vol. 11, no. 1, pp. 127–135, Jan. 2021. DOI: [10.1364/OME.411466](https://doi.org/10.1364/OME.411466).
- [86] V. Mikhailov, M. A. Melkumov, D. Inniss, A. M. Khagai, K. E. Riumkin, S. V. Firstov, F. V. Afanasiev, M. F. Yan, Y. Sun, J. Luo, G. S. Puc, S. D. Shenk, R. S. Windeler, P. S. Westbrook, R. L. Lingle, E. M. Dianov, and D. J. DiGiovanni, "Simple broadband bismuth doped fiber amplifier (BDFA) to extend O-band transmission reach and capacity," in *Proc. Opt. Fiber Commun. Conf.*, 2019, M1J.4. DOI: [10.1364/OFC.2019.M1J.4](https://doi.org/10.1364/OFC.2019.M1J.4).
- [87] J. Renaudier, A. Arnould, A. Ghazisaeidi, D. L. Gac, P. Brindel, E. Awwad, M. Makhsian, K. Mekhazni, F. Blache, A. Boutin, L. Letteron, Y. Frignac, N. Fontaine, D. Neilson, and M. Achouche, "Recent advances in 100+nm ultra-wideband fiber-optic transmission systems using semiconductor optical amplifiers," *J. Lightw. Technol.*, vol. 38, no. 5, pp. 1071–1079, May 2020. DOI: [10.1109/JLT.2020.2966491](https://doi.org/10.1109/JLT.2020.2966491).
- [88] M. F. C. Stephens, M. Tan, V. Gordienko, P. Harper, and N. J. Doran, "In-line and cascaded DWDM transmission using a 15dB net-gain polarization-insensitive fiber optical parametric amplifier," *Opt. Exp.*, vol. 25, no. 20, pp. 24 312–24 325, Oct. 2017. DOI: [10.1364/OE.25.024312](https://doi.org/10.1364/OE.25.024312).
- [89] T. Kobayashi, S. Shimizu, M. Nakamura, T. Umeki, T. Kazama, R. Kasahara, F. Hamaoka, M. Nagatani, H. Yamazaki, H. Nosaka, *et al.*, "Wide-band inline-

- amplified WDM transmission using PPLN-based optical parametric amplifier,” *J. Lightw. Technol.*, vol. 39, no. 3, pp. 787–794, 2021. DOI: [10.1109/JLT.2020.3039192](https://doi.org/10.1109/JLT.2020.3039192).
- [90] H. Masuda, M. Tomizawa, and Y. Miyamoto, “High-performance distributed raman amplification systems: Practical aspects and field trial results,” in *Proc. Opt. Fiber Commun. Conf.*, 2005, OThF5. DOI: [10.1109/OFC.2005.192926](https://doi.org/10.1109/OFC.2005.192926).
- [91] W. S. Pelouch, “Raman amplification: An enabling technology for long-haul coherent transmission systems,” *J. Lightw. Technol.*, vol. 34, no. 1, pp. 6–19, Jan. 2015. DOI: [10.1109/JLT.2015.2458771](https://doi.org/10.1109/JLT.2015.2458771).
- [92] H. Bissessur, C. Bastide, S. Dubost, and S. Etienne, “80×200 Gb/s 16-QAM unrepeated transmission over 321 km with third order Raman amplification,” in *Proc. Opt. Fiber Commun. Conf.*, 2015, W4E-2. DOI: [10.1364/OFC.2015.W4E.2](https://doi.org/10.1364/OFC.2015.W4E.2).
- [93] H. Masuda, “Review of wideband hybrid amplifiers,” in *Proc. Opt. Fiber Commun. Conf.*, vol. 1, 2000, pp. 2–4. DOI: [10.1109/OFC.2000.868354](https://doi.org/10.1109/OFC.2000.868354).
- [94] T. J. Xia, G. A. Wellbrock, M.-F. Huang, S. Zhang, Y.-K. Huang, D.-i. Chang, S. Burtsev, W. Pelouch, E. Zak, H. de Pedro, W. Szeto, and H. Fevrier, “Transmission of 400G PM-16QAM channels over long-haul distance with commercial all-distributed Raman amplification system and aged standard SMF in field,” in *Proc. Opt. Fiber Commun. Conf.*, 2014, Tu2B.1. DOI: [10.1364/OFC.2014.Tu2B.1](https://doi.org/10.1364/OFC.2014.Tu2B.1).
- [95] M. A. Iqbal, P. Harper, and W. Forysiak, “Improved design of ultra-wideband discrete Raman amplifier with low noise and high gain,” in *Proc. Adv. Photon. 2018*, 2018, NpTh1H-2. DOI: [10.1364/NP.2018.NpTh1H.2](https://doi.org/10.1364/NP.2018.NpTh1H.2).
- [96] U. C. De Moura, M. A. Iqbal, M. Kamalian, L. Krzaczanowicz, F. Da Ros, A. M. R. Brusin, A. Carena, W. Forysiak, S. Turitsyn, and D. Zibar, “Multi-band programmable gain Raman amplifier,” *J. Lightw. Technol.*, vol. 39, no. 2, pp. 429–438, Jan. 2020. DOI: [10.1109/JLT.2020.3033768](https://doi.org/10.1109/JLT.2020.3033768).
- [97] L. E. Nelson, X. Zhou, B. Zhu, M. F. Yan, P. W. Wisk, and P. D. Magill, “All-Raman-amplified, 73 nm seamless band transmission of 9 Tb/s over 6000 km of fiber,” *IEEE Photon. Technol. Lett.*, vol. 26, no. 3, pp. 242–245, Feb. 2013. DOI: [10.1109/LPT.2013.2291399](https://doi.org/10.1109/LPT.2013.2291399).
- [98] C. Doerr, L. Chen, T. Nielsen, R. Aroca, L. Chen, M. Banaee, S. Azemati, G. McBrien, S. Y. Park, J. Geyer, B. Guan, B. Mikkelsen, C. Rasmussen, M. Givchchi, Z. Wang, B. Potsaid, H. C. Lee, E. Swanson, and J. G. Fujimoto, “O, E, S, C, and L band silicon photonics coherent modulator/receiver,” in *Proc. Opt. Fiber Commun. Conf.*, 2016, Th5C.4. DOI: [10.1364/OFC.2016.Th5C.4](https://doi.org/10.1364/OFC.2016.Th5C.4).
- [99] C. Doerr and L. Chen, “Silicon Photonics in Optical Coherent Systems,” *Proceedings of the IEEE*, vol. 106, no. 12, pp. 2291–2301, Dec. 2018. DOI: [10.1109/JPROC.2018.2866391](https://doi.org/10.1109/JPROC.2018.2866391).
- [100] F. Hamaoka, “Ultra-wideband transmission and high-symbol rate signal handling technologies,” in *Proc. Opt. Fiber Commun. Conf.*, 2020, W3E.1. DOI: [10.1364/OFC.2020.W3E.1](https://doi.org/10.1364/OFC.2020.W3E.1).
- [101] W. Shi, Y. Tian, and A. Gervais, “Scaling capacity of fiber-optic transmission systems via silicon photonics,” *Nanophotonics*, vol. 9, no. 16, pp. 4629–4663, Oct. 2020. DOI: [10.1515/nanoph-2020-0309](https://doi.org/10.1515/nanoph-2020-0309).
- [102] M. Sena, Y. Cui, G. Fiol, B. Shariati, A. Napoli, J. K. Fischer, M. Schell, and R. Freund, “Performance Evaluation of InP-Based DP-IQ Modulators for Multi-band Transmission Systems,” in *Proc. 22nd Int. Conf. Transp. Opt. Netw.*, 2020, We.D2.5. DOI: [10.1109/ICTON51198.2020.9203554](https://doi.org/10.1109/ICTON51198.2020.9203554).
- [103] R. Halir, P. Cheben, J. M. Luque-González, J. D. Sarmiento-Merenguel, J. H. Schmid, G. Wangüemert-Pérez, D.-X. Xu, S. Wang, A. Ortega-Moñux, and Í. Molina-Fernández, “Ultra-broadband nanophotonic beamsplitter using an anisotropic sub-wavelength metamaterial,” *Laser & Photonics Reviews*, vol. 10, no. 6, pp. 1039–1046, Nov. 2016. DOI: [10.1002/lpor.201600213](https://doi.org/10.1002/lpor.201600213).
- [104] R. Emmerich, M. Sena, R. Elschner, C. Schmidt-Langhorst, I. Sackey, C. Schubert, and R. Freund, “Enabling S-C-L-Band Systems with Standard C-Band Modulator and Coherent Receiver using Nonlinear Predistortion,” in *Proc. Opt. Fiber Commun. Conf.*, 2021, F4D.7.
- [105] R. Elschner, R. Emmerich, C. Schmidt-Langhorst, F. Frey, P. W. Berenguer, J. K. Fischer, H. Grieser, D. Rafique, J.-P. Elbers, and C. Schubert, “Improving Achievable Information Rates of 64-GBd PDM-64QAM by Nonlinear Transmitter Predistortion,” in *Proc. Opt. Fiber Commun. Conf.*, 2018, p. M1C.2.
- [106] M. Sena, M. S. Erkilinc, T. Dippon, B. Shariati, R. Emmerich, J. K. Fischer, and R. Freund, “An Autonomous Identification and Pre-distortion Scheme for Cognitive Transceivers using Bayesian Optimization,” in *Proc. 46th Eur. Conf. Opt. Commun.*, 2020, Tu1D-7. DOI: [10.1109/ECOC48923.2020.9333408](https://doi.org/10.1109/ECOC48923.2020.9333408).
- [107] M. Sena, M. S. Erkilinc, T. Dippon, B. Shariati, R. Emmerich, J. K. Fischer, and R. Freund, “Bayesian Optimization for Nonlinear System Identification and Pre-Distortion in Cognitive Transmitters,” *J. Lightw. Technol.*, vol. 39, no. 15, pp. 5008–5020, Aug. 2021. DOI: [10.1109/JLT.2021.3083676](https://doi.org/10.1109/JLT.2021.3083676).
- [108] M. Sena, R. Emmerich, B. Shariati, J. K. Fischer, and R. Freund, “Evaluation of an Autonomous Digital Pre-distortion Scheme for Optical Multiband Systems,” in *Proc. Opt. Fiber Commun. Conf.*, 2021, F4D.5.
- [109] P. W. Berenguer, T. Rahman, A. Napoli, M. Nölle, C. Schubert, and J. K. Fischer, “Nonlinear digital pre-distortion of transmitter components,” *J. Lightw. Technol.*, vol. 34, no. 8, pp. 1739–1745, Apr. 2016. DOI: [10.1109/JLT.2015.2510962](https://doi.org/10.1109/JLT.2015.2510962).
- [110] G. Khanna, B. Spinnler, S. Calabro, E. De Man, U. Feiste, T. Drenski, and N. Hanik, “A Memory Polynomial Based Digital Pre-Distorter for High Power

- Transmitter Components,” in *Proc. Opt. Fiber Commun. Conf.*, 2017, p. M2C.4.
- [111] S. J. B. Yoo, “Wavelength conversion technologies for WDM network applications,” *J. Lightw. Technol.*, vol. 14, no. 6, pp. 955–966, Jun. 1996. DOI: [10.1109/50.511595](https://doi.org/10.1109/50.511595).
- [112] K. Inoue, “Four-wave mixing in an optical fiber in the zero-dispersion wavelength region,” *J. Lightw. Technol.*, vol. 10, no. 11, pp. 1553–1561, Nov. 1992. DOI: [10.1109/50.184893](https://doi.org/10.1109/50.184893).
- [113] S. Watanabe, S. Takeda, and T. Chikama, “Interband wavelength conversion of 320 Gb/s (32×10 Gb/s) WDM signal using a polarization-insensitive fiber four-wave mixer,” in *Proc. 24th European Conf. Opt. Commun.*, 1998, 83–87 vol.3. DOI: [10.1109/ECOC.1998.731208](https://doi.org/10.1109/ECOC.1998.731208).
- [114] T. Kato, S. Watanabe, T. Yamauchi, G. Nakagawa, H. Muranaka, Y. Tanaka, Y. Akiyama, and T. Hoshida, “Whole band wavelength conversion for wideband transmission,” in *Proc. Opt. Fiber Commun. Conf.*, 2021, F1B.1.
- [115] A. Shamshooli, C. Guo, F. Parmigiari, X. Li, Y. Akasaka, P. Palacharla, and M. Vasilyev, “Emerging applications of wavelength conversion,” in *Proc. 2021 IEEE Photon. Conf.*, 2021, ThE2.1. DOI: [10.1109/IPC48725.2021.9592892](https://doi.org/10.1109/IPC48725.2021.9592892).
- [116] M. S. Sarwar, T. Sakamoto, T. Kato, and T. Hoshida, “Translambda: A multi-band transmission system and its realization, practical applications and use cases in optical networks,” in *Proc. Opt. Fiber Commun. Conf.*, 2020, M2G.6. DOI: [10.1364/OFC.2020.M2G.6](https://doi.org/10.1364/OFC.2020.M2G.6).
- [117] H. Kawahara, M. Nakagawa, T. Seki, and T. Miyamura, “Experimental demonstration of wavelength-selective band/direction-switchable multi-band OXC using an inter-band all optical wavelength converter,” in *Proc. 46th Eur. Conf. Opt. Commun.*, 2020, Tu1H–5. DOI: [10.1109/ECOC48923.2020.9333270](https://doi.org/10.1109/ECOC48923.2020.9333270).
- [118] M.-C. Ho, K. Uesaka, M. Marhic, Y. Akasaka, and L. G. Kazovsky, “200-nm-bandwidth fiber optical amplifier combining parametric and Raman gain,” *J. Lightw. Technol.*, vol. 19, no. 7, pp. 977–981, Jul. 2001. DOI: [10.1109/50.933292](https://doi.org/10.1109/50.933292).
- [119] S. Takasaka, “Techniques for optical parametric amplification using highly nonlinear fiber,” in *Proc. 2019 IEEE Photon. Conf.*, 2019, p. MC2.4. DOI: [10.1109/IPCon.2019.8908421](https://doi.org/10.1109/IPCon.2019.8908421).
- [120] T. Torounidis, P. A. Andrekson, and B.-E. Olsson, “Fiber-optical parametric amplifier with 70-dB gain,” *IEEE Photon. Technol. Lett.*, vol. 18, no. 10, pp. 1194–1196, May 2006. DOI: [10.1109/LPT.2006.874714](https://doi.org/10.1109/LPT.2006.874714).
- [121] M.-C. Ho, M. E. Marhic, K. Y. K. Wong, and L. G. Kazovsky, “Narrow-linewidth idler generation in fiber four-wave mixing and parametric amplification by dithering two pumps in opposition of phase,” *J. Lightw. Technol.*, vol. 20, no. 3, pp. 469–476, Mar. 2002. DOI: [10.1109/50.988996](https://doi.org/10.1109/50.988996).
- [122] T. Kato, S. Watanabe, T. Tanimura, R. Elschner, C. Schmidt-Langhorst, C. Schubert, and T. Hoshida, “Fiber-optic frequency shifting of THz-range WDM signal using orthogonal pump-signal polarization configuration,” in *Proc. Opt. Fiber Commun. Conf.*, 2018, M3E.3. DOI: [10.1364/OFC.2018.M3E.3](https://doi.org/10.1364/OFC.2018.M3E.3).
- [123] M. A. Foster, A. C. Turner, R. Salem, M. Lipson, and A. L. Gaeta, “Broad-band continuous-wave parametric wavelength conversion in silicon nanowaveguides,” *Opt. Exp.*, vol. 15, no. 20, pp. 12 949–12 958, Oct. 2007. DOI: [10.1364/OE.15.012949](https://doi.org/10.1364/OE.15.012949).
- [124] C. J. Krückel, V. Torres-Company, P. A. Andrekson, D. T. Spencer, J. F. Bauters, M. J. R. Heck, and J. E. Bowers, “Continuous wave-pumped wavelength conversion in low-loss silicon nitride waveguides,” *Opt. Lett.*, vol. 40, no. 6, pp. 875–878, Mar. 2015. DOI: [10.1364/OL.40.000875](https://doi.org/10.1364/OL.40.000875).
- [125] C. Lacava, S. Stankovic, A. Z. Khokhar, T. D. Bucio, F. Y. Gardes, G. T. Reed, D. J. Richardson, and P. Petropoulos, “Si-rich silicon nitride for nonlinear signal processing applications,” *Scientific Reports*, Feb. 2017. DOI: [10.1038/s41598-017-00062-6](https://doi.org/10.1038/s41598-017-00062-6).
- [126] R. F. Cregan, B. J. Mangan, J. C. Knight, B. T. A. P. S. Russell, P. J. Roberts, and D. C. Allan, “Single-mode photonic band gap guidance of light in air,” *Science*, vol. 285, no. 5433, pp. 1537–1539, 1999. DOI: [10.1126/science.285.5433.1537](https://doi.org/10.1126/science.285.5433.1537).
- [127] P. Poggiolini and F. Poletti, “Opportunities and challenges for long-distance transmission in hollow-core fibres,” *J. Lightw. Technol.*, vol. 40, no. 6, pp. 1605–1616, 2022. DOI: [10.1109/JLT.2021.3140114](https://doi.org/10.1109/JLT.2021.3140114).
- [128] A. Nespola, S. R. Sandoghchi, L. Hooper, M. Alonso, T. D. Bradley, H. Sakr, G. T. Jasion, E. Numkam Fokoua, S. Straullu, F. Garrisi, G. Bosco, A. Carena, A. M. Rosa Brusin, Y. Chen, J. R. Hayes, F. Forghieri, D. J. Richardson, F. Poletti, and P. Poggiolini, “Ultra-long-haul WDM transmission in a reduced inter-modal interference NANF hollow-core fiber,” in *Proc. Opt. Fiber Commun. Conf.*, 2021, post-deadline paper F3B.5.
- [129] S. Ramachandran, J. Nicholson, S. Ghalmi, and M. Yan, “Measurement of multipath interference in the coherent crosstalk regime,” *IEEE Photon. Technol. Lett.*, vol. 15, no. 8, pp. 1171–1173, Aug. 2003. DOI: [10.1109/LPT.2003.814880](https://doi.org/10.1109/LPT.2003.814880).





**Takeshi Hoshida** (S'97-M'98-SM'20) received his B.E., M.E., and Ph.D. degrees in electronic engineering from the University of Tokyo, Tokyo, Japan, in 1993, 1995, and 1998, respectively.

Since he joined Fujitsu Laboratories Ltd., Kawasaki, Japan, in 1998, he has been engaged in research and development of dense wavelength division multiplexing optical transmission systems. From 2000 to 2002, he was with Fujitsu Network Communications, Inc., Richardson, Texas. Since 2007, he has been with Fujitsu Limited, Kawasaki, Japan and he currently heads Fujitsu's optical transmission research efforts.

Dr. Hoshida received Commendation for Science and Technology by the Ministry of Education, Culture, Sports, Science and Technology (Awards for Science and Technology in Development Category) in 2020 and the Japan Patent Office Commissioner Award of the National Commendation for Invention in 2020. He is a senior member of the Institute of Electronics, Information and Communication Engineers (IEICE) and a member of the Japan Society of Applied Physics (JSAP).



**David T. Neilson** (M'96-F'10) received the B.Sc. and Ph.D. degrees in physics from Heriot-Watt University, Edinburgh, U.K., in 1990 and 1993, respectively. He is the Group Leader for Optical Transmission Research at Nokia Bell Labs, in NJ USA, and a Bell Labs Fellow. The departments in the group conduct research into optical systems for terrestrial and undersea, including ultra-high baud rates, modulation formats and coding and the use of space division multiplexing, for scaling system capacities. He joined Bell-Labs in 1998, where he

has lead research on optical switching systems and on opto-electronic integration. This includes MEMS and LCoS for wavelength selective switches and optical cross-connects; InP and Silicon photonics. From 1993 to 1996, he was a Postdoctoral Researcher working on free-space optical interconnect and switching systems with Heriot-Watt. From 1996 to 1998, he was a Visiting Scientist with NEC Research, Princeton, NJ, researching optical interconnects for high-performance computing systems. He has authored more than 200 publications, patents, and short courses, on both devices and systems in the field of optical interconnects and switching. He has served on and chaired several IEEE-LEOS, OSA, and SPIE conference programs in the field of optical interconnects and switching.



**Vittorio Curri** received the Laurea degree in electrical engineering in 1995, and the Scientific Doctoral degree in optical communications in 1999, both from Politecnico di Torino (PoliTo), Italy. He is a founder member of the OptCom group and PhotonLab at PoliTo. He is currently a Full Professor with the Department of Electronics and Telecommunications, PoliTo. He has been a Visiting Researcher at the Stanford University and UC at Santa Barbara. His major research interests are in fiber transmission modeling, including nonlinearities, transmitter and

receiver optimization, design strategies for optical links, Raman amplification and simulation and modeling of optical communication systems. He is one of the promoters of using multi-band transmission in single-mode fibers and investigates on the topic within the H2020 ETN Wideband Optical Networks. Prof. Curri is also active in the analysis of the impact of physical layer on networking for planning and control of open and disaggregated optical networks, including AI techniques, and he is the Scientific Chair of the GNPY open source project within the consortium Telecom Infra Project. Prof. Curri is an IEEE Senior Member, and Optica member and is the co-author of more than 330 scientific publications.



**Wladek Forysiak** (M'03) received the B.Sc. and Ph.D. degrees in physics from Imperial College, London, and Heriot-Watt University, Edinburgh, UK, in 1985 and 1989, respectively.

He has a research background in nonlinear photonics, optical solitons, and high-speed optical fibre communication systems. In 2000, he co-founded Marconi-Solstis and spent 15 years in WDM system-related product development with marconi, Ericsson, and Oclaro. He has served as a Royal Society Industry Fellow and an EPSRC Manufacturing Fellow,

and is presently the EFFECT Photonics / Royal Academy of Engineering Research Chair in Highly Integrated Coherent optical fibre Communications. His current research interests include wideband optical fibre communication systems, optical devices, transceivers and subsystems, and the impact and mitigation of device and fibre nonlinearities.



**Lidia Galdino** received the M.Sc. and Ph.D. degrees in electronic and electrical engineering from the University of Campinas, Campinas, Brazil, in 2008 and 2013, respectively.

She subsequently joined the Optical Networks Group, University College London (UCL) to work as a Research and Senior Research Associate. She is currently a Lecturer and a Royal Academy of Engineering Research Fellow at UCL on the topic of "Capacity-approaching, Ultra-Wideband Nonlinear Optical Fibre Transmission System". Dr Galdino

has been elected to the Board of Governors for the IEEE Photonics Society and has served in the Technical Program Committees of several conferences, including ECOC, OFC, IEEE IPC. She is author or co-author of more than 100 scientific publication. She was a co-recipient of the RAEng Colin Campbell Mitchell Award in 2015 for pioneering contributions to optical communications technology and named as one of the 2017 "Top 50 Women in Engineering under 35" by The Telegraph and Women in Engineering Society which features the U.K.'s top rising female stars of engineering.



**Johannes K. Fischer** (S'04-M'09-SM'15) received the Dipl.-Ing. and Dr.-Ing. degrees in electrical engineering from TU Berlin, Berlin, Germany, in 2003 and 2009, respectively.

In 2010, he joined the Fraunhofer Institute for Telecommunications, Heinrich Hertz Institute, Berlin, where he is currently heading a research group on digital signal processing within the Department of Photonic Networks and Systems. He is author or coauthor of more than 120 articles and a book chapter. His research interests include

advanced modulation formats, digital signal processing and machine learning for optical systems.

Dr. Fischer is a senior member of IEEE and a member of the VDE, where he serves in working group KT 3.1 "Modelling of Photonic Components and Systems" of the Information Technology Society. He has also served in the Technical Program Committees of OECC and OFC.





**Tomoyuki Kato** (S'05–M'06) received the B.E., M.E., and Dr.Eng. degrees in electronic engineering from Yokohama National University, Yokohama, Japan, in 2001, 2003, and 2006, respectively.

From 2006 to 2009, he was a Research Associate with the Precision and Intelligence Laboratories, Tokyo Institute of Technology. Since he joined Fujitsu Laboratories Ltd., Kawasaki, Japan, in 2009, he has been engaged in the research of nonlinear optical signal processing for dense wavelength division multiplexing optical transmission systems. Since 2019,

he has been with Fujitsu Limited, Kawasaki, Japan.



**Pierluigi Poggiolini** received his M.S. degree cum laude in 1988 and his Ph.D. degree in 1993 from Politecnico di Torino, Italy. From 1988 to 1989 he was with the Italian State Telephone Company research center CSELT. From 1990 to 1995 he was a Visiting Scholar and then a Post-Doctoral Fellow at the Optical Communications Research Laboratory of Stanford University. Since 2010 he has been a Full Professor at Politecnico di Torino. He was an elected member of the Academic Senate (2005-2010) and of the Board of Directors (2016-2020) of Politecnico di

Torino. He was Technical Co- Chair of the ECOC conference in 2010. He has published over 250 papers in leading journals and conferences. He is a co-author of two papers, published in 2011 and 2012, that have received the Journal of Lightwave Technology Best Paper Award. He is an OPTICA and IEEE Fellow. His current research interests include long-haul coherent transmission systems, non-linear fiber effects, modeling and simulation of optical communications systems, hollow-core fiber transmission systems.